*Article*

# On the Role of the Building Envelope on the Urban Heat Island Mitigation and Building Energy Performance in Mediterranean Cities: A Case Study in Southern Italy

Alessandra Martinelli, Francesco Carlucci [ID] and Francesco Fiorito *[ID]

Department of Civil, Environmental, Land, Building Engineering and Chemistry, Polytechnic University of Bari, 70125 Bari, Italy; alessandra.martinelli@poliba.it (A.M.); francesco.carlucci@poliba.it (F.C.)
* Correspondence: francesco.fiorito@poliba.it

**Abstract:** The urban heat island (UHI) effect is one of the largest climate-related issues concerning our cities due to the localized temperature increase in highly urbanized areas. This paper aims to investigate the impact of UHI mitigation techniques in promoting climate resilience, by reducing urban air temperatures and cooling energy consumption in buildings. To this end, four mitigation solutions regarding the building envelope—green roofs, green walls, cool roofs, and cool walls—were investigated for the city of Bari in Southern Italy and compared with the current baseline scenario. Hence, five scenarios were simulated—using the ENVI-met microclimate software—during three representative summer days, and the resulting microclimate changes were assessed. Based on these analyses, new climate files—one for each scenario—were generated and used as input to run energy simulations in EnergyPlus to estimate the building cooling consumption. Coupling the microclimate and the consumption outcomes, the mitigation strategies were evaluated from both an urban and building point of view. The study shows that urban characteristics, mainly geometry and materials, are crucial for the UHI phenomenon. All the applied technologies seem to be effective. However, green walls proved to be more efficient in reducing outdoor temperatures (1 °C reduction in daily temperatures), while cool walls performed better in reducing cooling energy consumption, with an overall saving of 6% compared to the current scenario.

**Keywords:** urban heat island; mitigation technologies; energy consumption; Mediterranean climate; sustainable design; environmental design

## 1. Introduction

During the 21st century, extreme weather and climate-related events have directed the attention of researchers toward climate change-related challenges [1]. Climate change is a global phenomenon; its mitigation through the reduction in greenhouse gas emissions requires a global effort, but the impacts of a changing climate are localized. Climate change is a risk factor linked to human behavior that may strongly influence the performance of the built environment by introducing new vulnerabilities, modifying the performance and the efficiency of technological systems by increasing energy demand and reducing users' comfort [2,3]. Vulnerability is exacerbated by increasing urbanization and the exodus of the population from rural to urban and suburban areas.

Recent analyses [1] confirm that extreme weather and climate events can pose significant risks to societies and ecosystems, and that the effects of human-induced climate change can already be recognized in current events. Cities play a pivotal role in response to climate change, especially in a highly urbanized continent like Europe, where climate-adapted planning and urban design can substantially reduce future damage related to changing climate [4].

A study by Tapia et al. [5] assessed the vulnerability of over 500 European cities based on specific indicators (human and natural capital, governance and institutions, socio-

economic conditions, and built environment), finding that highly vulnerable cities are mainly located in Central Europe, Germany, Estonia, Romania, and Latvia. In terms of vulnerability to heat waves, the most affected towns are those located mainly in the Southern and Central EU and the Baltic republics due to a combination of elderly populations, small house sizes, and high levels of air pollution. Moreover, climate projections in Europe show a rise in temperature across the continent: the highest seasonal warming occurs in summer in Southern Europe and winter in Northern Europe. In a high-emission scenario, Lehner et al. [6] predicted that by the end of the century, 90% of summers in Southern, Central, and Northwestern Europe would be warmer than any summer from 1920 to 2014. The most severe health risks identified are localized within Southern Europe [7] and the Mediterranean coasts due to densely populated urban centers. To date, high temperatures and heat waves have claimed more victims in Europe than any other weather-related disaster.

In particular, the inevitable rise in temperatures due to climate change is further visible and exacerbated in cities because of the urban heat island (UHI) effect, which is the most widely documented climatological effect resulting from the anthropogenic transformation of the natural environment [8]. This phenomenon causes a difference in temperature between urban areas and their rural surroundings. It is caused by the increased heat capacity, the imperviousness of urban surfaces that inhibits evaporative cooling, and is exacerbated by anthropogenic heat sources such as space heating and cooling, transportation, and industrial processes [9,10]. Urban and local meteorological characteristics, urban materials, and the presence or lack of green areas also heavily influence the UHI's intensity, which widely varies depending on the European town and increases during hot periods [11]. Urban warming and UHI produce severe energy and environmental impacts on cities and threaten the quality of citizens' lives [12]. Understanding and reducing the cities' vulnerability is the key to address the problems associated with rising temperatures, UHI, and heat-related mortality in cities.

Moreover, high outdoor temperatures lead to higher indoor temperatures that could be dangerous for the most vulnerable population categories [13]. At the same time, high indoor temperatures lead to an increase in the energy demand. Especially in summer, energy consumption due to cooling increases, internal and external thermal comfort worsen, and harmful pollutants like the tropospheric ozone severely affect citizens' health conditions [14]. In this regard, the 2019 EEA report states that peak electricity demand for cooling will increase throughout Europe, especially in Italy, France, and Spain [15]. Since this is also dependent on the building design [16,17], building-level adaptation measures are essential to mitigate these risks.

Furthermore, because of the expected future emissions related to the city growth and energy demand management, critical questions like urbanization, urban expansion, and urban development need to be examined [11]. Poor urban design can thus amplify the impacts of climate change, and, in the future, buildings designed to face certain thermal conditions may have to operate in drier and warmer climates.

For these reasons, it is crucial to delve into the analysis and development of new and more efficient mitigation strategies and technologies for the UHI effect [18]. A resilient approach is required to achieve the transformation and regeneration of the existing environment. In this regard, the effectiveness of adaptation measures addressing heat is measured by various indicators, including human comfort, outdoor and indoor temperatures, and energy-saving levels [4].

Some of the most effective mitigation technologies applicable to buildings and to the urban context rely on nature-based solutions [19] and on the use of cool materials [20]. The former can reduce the heat storage capacity of urban surfaces and air temperature by increasing the evapotranspiration and shading effects [21]; the latter can reduce temperatures through higher solar reflectance and infrared emittance [21].

Therefore, cities are clearly the main field of experimentation for innovative and climate-resilient design principles and methods. This research fits in this framework and continues the previous survey carried out by Martinelli et al. [22]. In particular, this study

aimed at investigating the urban heat island phenomenon in a Mediterranean coastal city (Bari) in Southern Italy. The first part investigated the effects on the urban microclimate, deriving from specific UHI mitigation technologies on the urban microclimate through climate simulations conducted with ENVI-met. Hence, new climate files were created and used as input weather files for building energy simulations. The goal was to understand how effectively different mitigation technologies help to reduce the UHI phenomenon and to verify the indirect effects of mitigation in terms of the reduction in the cooling consumption of buildings during the summer period. To introduce these topics, the following subsections describe the state-of-the-art mitigation technologies adopted in this study and the impact of the UHI effect on the building energy consumption.

### 1.1. The Energy Impact of the Urban Heat Island Effect

As explained before, the UHI effect can impact indoor comfort, leading, as consequence, to an increase in cooling consumption [23]. In particular, the most documented effect is related to a significant increase in the peak global electricity demand for HVAC systems and a significant decrease in the performance of air conditioning systems. It typically depends on the magnitude of the urban warming, local climate conditions, and HVAC systems [11]. Akbari reported that the peak electricity load in U.S. cities with populations larger than 100,000 inhabitants could increase by 1.5–2.0% for every 0.45 °C increase in temperature [24]. In parallel, Santamouris et al. found that the cooling load in downtown Athens (Greece) is double that of the surrounding region; specifically, the peak electricity demand triples, while the heating load may be reduced to 30–50% in the urban area [25]. Moreover, further studies underlined that offices and individual households increasingly use air conditioning—especially in the Mediterranean area—and such a trend is assumed to continue [26].

Since the increase in urban temperatures, along with the resulting increasing risk of overheating and indoor thermal discomfort, is greatly influenced by the sensible heat flux and energy storage of the construction materials [2,27], the UHI mitigation technologies considered in this study—as previously illustrated—can also produce co-benefits in terms of the energy-saving rates of buildings [13,28].

### 1.2. Mitigation Technologies and Mitigation Potential

The last report of the IPCC (Intergovernmental Group on Climate Change) emphasizes human influence as the dominant cause of climate change [1]. Climate change is usually linked to resilience, i.e., the capacity of a system to absorb disturbance and reorganize while changing to retain substantially the same function, structure, identity, and feedback. It is thus essential to study the urban microclimate to understand the interaction between urban elements, climate, and comfort, optimize design choices within cities, and include them as solutions to climate change and as an opportunity to develop strategies for related adaptation and mitigation.

The materials used in the urban environment play a significant role in the urban thermal balance: they absorb the incident solar radiation, dissipate into the atmosphere a percentage of the heat absorbed through radiative exchanges, and consequently affect the ambient temperature [29]. For this reason, the focus of this paper is the mitigation potential of different materials, and two major promising groups of mitigation strategies were identified and investigated:

- Increasing evapotranspiration: This strategy includes nature-based solutions (NBSs) through the intensive use of urban greenery (such as urban parks or water-permeable pavements) and green envelopes applied to buildings.
- Increasing solar reflectance (albedo): This strategy includes the use of materials with high solar reflectance (and high thermal emittance) to keep surfaces cool. These materials—known as cool materials—can be adopted in both the building envelope and outdoor pavements.

In a report published by the European Commission [30], the NBSs are defined as the interventions inspired by nature that uses "the characteristics and processes of the whole system, such as its ability to store carbon and adjust the water flow". Moreover, NBSs "address a series of economic, social and environmental challenges in a sustainable way, such as disaster risk reduction, improving human and social well-being inclusive green growth" [30].

In this work, nature-based solutions refer to those urban interventions that use nature—and its processes—to mitigate climate change and UHI effects, while providing several further benefits in terms of environmental quality, human health and well-being, energy-saving, urban regeneration capacity, improved livability, etc. Recent studies have shown that nature-based solutions may mitigate climate change more efficiently than engineering and technological solutions [31].

The thermal impacts of green surfaces are essential in the urban environment, especially in urban canyons [32,33]. Indeed, solar radiation is absorbed by urban surfaces and is entrapped, causing an increase in the surface temperature; then, due to the lack of proper airflow that would allow for recirculation, the air temperatures rise [34]. Through evapotranspiration, vegetation cools the air using heat to evaporate water and reduce peak air temperatures in summer. From a quantitative point of view, a previous study conducted by Brahimi et al. [35] has highlighted that—by implementing green surfaces in a semi-arid climate—the temperature decrease stands at nearly 0.5 °C at 8:00, peaking at 1.05 °C at 13:00. These benefits progressively increase during the morning and slowly fade during night [35]. Upon looking at the concept of green roofs in more detail, the average temperature decrease reported in the existing literature is between 0 and 2 °C, with a median value near 0.2 °C, whereas the maximum temperature drop of the ambient temperature is estimated to be between 0 and 3 °C, with a median value around 0.6 °C [36]. Clearly, the cooling potential of green roofs depends on the building height, as increasing the distance between the street level and the roof reduces the influence of the greenery on the urban microclimate. It follows that the cooling potential at street level tends to 0 when high-rise buildings are considered [36]. Considering the implementation of green walls, a review conducted by Susca et al. [37] has highlighted that the UHI effect can be mitigated in different climates thanks to this strategy. In particular, by implementing the green wall on a single building façade, the median decrease in air temperature reaches nearly 1 °C, with the highest benefits recorded on the southern façade except for the Cwa climate, where the highest benefits are recorded on the western exposure. Moreover, overall, the green wall strategy can mitigate the UHI effect up to nearly 5 °C in all the investigated climate zones. Furthermore, the studies conducted at the scale of buildings and canyon streets have shown the positive impact of green walls in summer in reducing heat loads, radiant temperature, and air temperature inside buildings while reducing the outdoor temperature [38]. In particular, previous studies conducted in France have demonstrated that the operational temperature within the building block can be dropped to as much as 5 °C by implementing green walls [38]. From an energy point of view, the increase of 1 °C of the air temperature leads to an increase in daily cooling demand of nearly 12% and a decrease of 8% in heating demand [39]. It follows that green walls can lead to significant energy-savings in several climates on both heating and cooling, which can be reduced to 16.5% and 51%, respectively [37].

Moving to the so-called "cool materials", building envelopes and open spaces covered by these materials can reflect a significant part of solar radiation and dissipate the heat absorbed through radiation. Cool materials contribute to increasing the urban albedo, maintaining lower surface temperatures, representing an effective solution to mitigate urban heat islands [40,41]. Over the last few years, a considerable number of studies on solar reflective materials have been carried out [42]. This spread has contributed to the development of innovative materials and techniques with advanced radiative properties and better thermal characteristics, leading to significant UHI mitigation potential [43]. For example, the application of cool road surfaces and reflective roofs in Geneva (Switzerland)

showed a reduction in yearly mean surface temperature of 2.5 °C, and reaching 5.0 °C in July [44]. Considering all the building technologies, cool roofs and cool walls are the most widespread solutions adopted according to these mitigation strategies. Similarly to what was already described for the green roofs, the effectiveness of the cool roofs strictly depends on the buildings' height as their contribution is negligible when applied on high-rise buildings. However, on average, an increase of nearly 10% of the roof albedo corresponds to an average temperature drop of 0.23 °C and a maximum temperature reduction of 0.62 °C [36]. On the contrary, the contribution of cool walls in the outdoor air reduction is limited to 0.1 °C while considering the energy demand; the results are strictly dependent on the specific boundary conditions (occupancy, urban context, etc.) [45].

## 2. Materials and Methods

Studies regarding the UHI effect have shown that this phenomenon is heavily dependent on geographic location, meteorological conditions of the urban area [46], and urban morphology [47]. Since the uncontrollable factors influencing the urban heat island cannot be modified, and the configuration of existing urban centers is now consolidated, the attention of this study is focused on those urban interventions that can be easily adapted and implemented in existing contexts. All the technologies investigated refer to the building envelope; hence, this study works on both urban and building scales. To this end, both microclimatic (ENVI-met version 4.4.3) and building energy software (EnergyPlus version 9.3.0) were used, with each requiring specific settings, input data, and considerations, which are described in detail in the following subsections; however, the overall approach adopted can be summed up in four main macro-steps, where each one is described in the following subsections:

1. Analysis of the site location and climate characteristics;
2. Urban microclimate modeling in ENVI-met and use of actual climate data;
3. Implementation of the mitigation technologies;
4. Creation of new weather files and modeling of the building in EnergyPlus.

Before delving into each subsection, it is worth highlighting that the conducted study is a simulation-based research and the main sources of uncertainty are limited to the weather station's sensitivity, the modeling, and the software's reliability. Considering the weather station sensitivity, the reported data are quite reliable with an error of ±0.1 °C for air temperature, ±0.1% for relative humidity, and ±0.1 m/s for wind speed. These small uncertainties are the same for all the simulations conducted, are limited only to the initial settings of the simulations, and are not directly taken into account in the final comparisons, which were conducted considering only the third simulated day. Considering further potential input data inaccuracies related to the modeling itself (e.g., materials, vegetation) these values are not directly measured or quantified but are basically reference values available in the scientific literature. Although these values can change according to the specific solutions adopted, using the same reference values in all the scenarios considered still allows us to conduct reliable comparisons between the mitigation strategies. Moreover, considering the deterministic approach of the simulation engine and the limited modeling uncertainty—as better explained below—all the simulations conducted consider the same starting uncertainty, which causes, in turn, the same limited output uncertainty. Therefore, considering that the main output of this study is a comparison between different strategies and not the exact value of an environmental parameter, these small input uncertainties can be considered negligible for the purpose of the final output comparison.

With regard to software reliability, Envi-Met is one of the most reliable dynamic simulation tools for microclimate analysis [48], and due to its high computational demand, it has difficulty in conducting sensitivity and validation analyses, which are rarely conducted in these studies and, when conducted, are limited to air temperature [49]. Previous studies have already highlighted that the temperature changes related to the mitigation strategies are an order of magnitude larger than the errors related to the geometric modeling of the urban area [50]. Moreover, Envi-MET is particularly reliable for comparing relative change

in parameters rather than assessing the absolute values [51], which is the main purpose of this study.

Similar considerations can be made for energy modeling, as EnergyPlus is one of the most reliable and adopted software thanks to its great analytical depth. Also, in this case, the analyses conducted are in relation to a widely shared reference model rather than to a specific building. By using a representative reference building, no characteristics are directly measured on site, but they are simply a realistic starting point to compare different strategies which refer to the same baseline model.

## 2.1. Site Location and Climate Characteristics

This study was carried out in the city of Bari (41.12 N, 16.87 E), located in the eastern coast of Southern Italy. This city is characterized by a typical temperate climate of Mediterranean cities with mild winters and hot summers. A specific area for the analyses was chosen based on a previous study conducted by Martinelli et al. [22] that identified—starting from the air temperatures recorded at fixed meteorological stations—the area characterized by the highest UHI effect. Based on the air temperature data collected, the urban heat island intensity led to identifying Bari CUS and Bari Cavour as rural and urban areas, respectively (Figure 1c). The resulting differences in daily (Figure 1a) and monthly (Figure 1b) air temperatures of urban and rural locations, within a year, are reported in Figure 1.
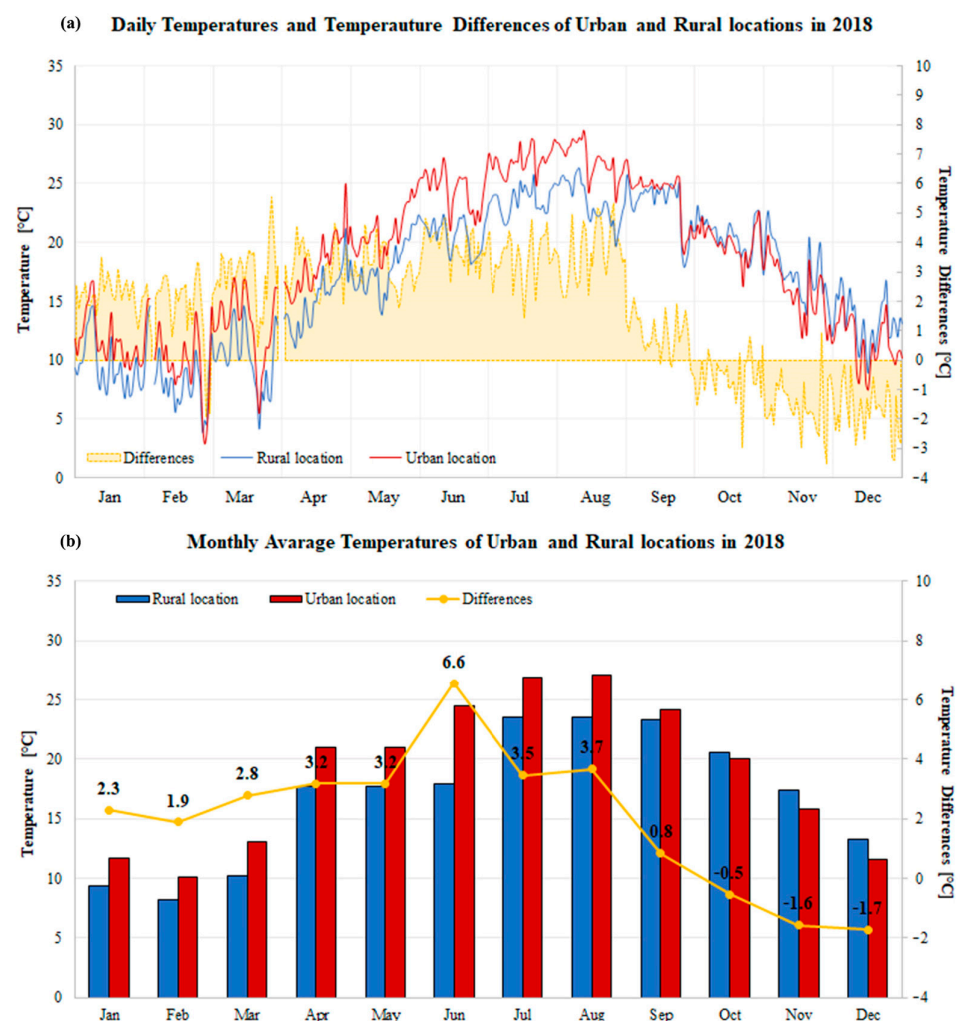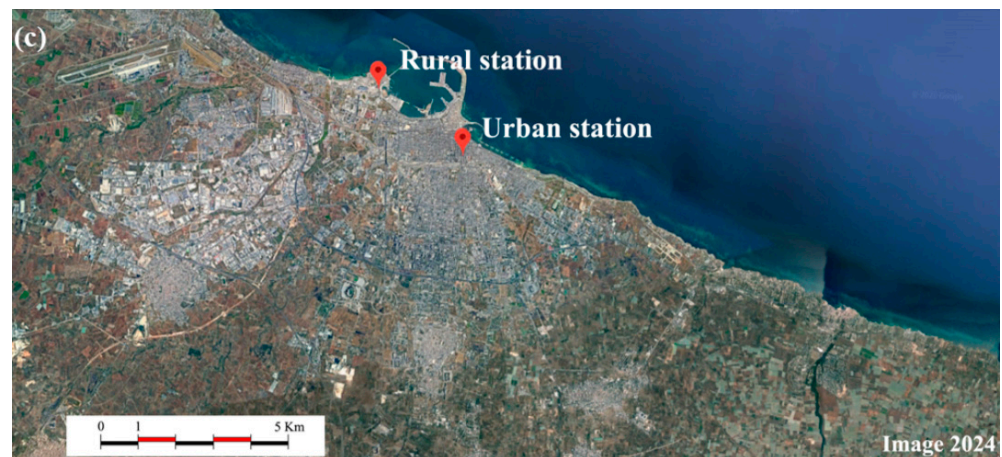


**Figure 1.** *Cont.*

**Figure 1.** The differences in (**a**) daily and (**b**) monthly air temperatures of urban and rural locations in 2018, and (**c**) locations of urban and rural weather stations.

The daily difference in temperature between the urban and reference stations fluctuates throughout the period with a maximum of 5.5 °C on the 28th of March and a minimum of −3.4 °C on the 28th of December. The average difference for the whole period of measurements is almost 2.0 °C. On a monthly basis (Figure 1b), the UHI intensity increases after May and reaches its maximum value of 6.6 °C in June, decreasing after August.

The area where UHI occurs more intensely is the one closest to the city center, where urban geometry, the lack of vegetation, the urban fabric, and the anthropogenic heat produced contribute to amplifying the UHI compared to the areas furthest from the city center. In particular, the selected area is a square-shaped area (250 m × 250 m) in the city center, in the Corso Cavour (main road) area, a densely built area with a northwestern orientation (Figure 2). The area has a very dense regular square pattern consisting of several buildings, of variable heights ranging from 15 m to about 40 m approximately, that are very close to each other and interspersed with narrow streets not exceeding 15 m in width. Green elements are almost absent here, resulting in a compact midrise Local Climate Zone (LCZ 2).
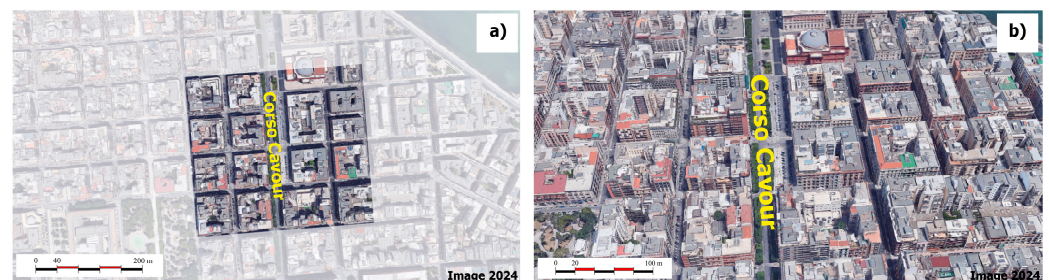


**Figure 2.** Google Earth image of (**a**) Corso Cavour area selected for modeling and simulation, and (**b**) an overhead view of the study area.

### 2.2. Urban Microclimate Modeling

Climate can be analyzed at the macro level (whole-planet scale), meso-level (city or country scale), and at the micro level (single-building or neighborhood scale). At this stage, this study is focused on the microscale, and the simulation software ENVI-met was adopted as reference. ENVI-met is a three-dimensional modeling tool used to simulate the surface–plant–air interaction, mainly for urban environments. The model considers a set of parameters (air temperature, surface temperature, wind speed, direction, etc.) and returns as output microclimate physical parameters, simulating heat and water vapor exchanges and mass transfers. This software allows us to analyze the effects of small-scale changes in urban design (e.g., trees, greening, new buildings) on the microclimate.

The geometric model was initially digitized in ENVI-met with the current existing configuration of buildings and green spaces (Figure 3).
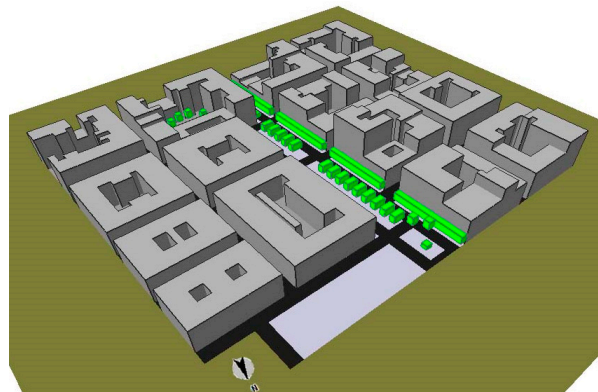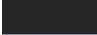


**Figure 3.** Input file model: 3D view.

The area was rendered in $100 \times 100 \times 30$ (x-y-z) grids, considering the following spacing: dx = 5.00 m, dy = 5.00 m, dz = 3.00 m. Therefore, the maximum height of the model is 90 m (30 cells $\times$ 3.00 m). Considering that the buildings' heights range between 8 and 40 m, the maximum height is at least twice the height of the tallest building; this characteristic allows us to achieve the numerical stability required by the software [52]. With reference to vegetation, 5.00 m high cylindric trees with medium trunks and dense foliage were used. From a material point of view, the soil was modeled with traditional concrete pavement for the pedestrian areas and asphalt for roads whose characteristics are reported in Table 1.

**Table 1.** Physical characteristics of basic materials.

| Element | Material | Color | Roughness Length | Albedo | Emissivity |
|---|---|---|---|---|---|
| Streets | Asphalt road | | 0.01 | 0.2 | 0.9 |
| Pavements | Pavement (concrete), used/dirty | | 0.01 | 0.4 | 0.9 |
| Building envelopes | Default wall; moderate insulation | | 0.02 | 0.5 | 0.9 |

This configuration was adopted as the starting point while the starting microclimate conditions (temperature, humidity, wind speed, etc.) were set using hourly real-time monitored data provided by ARPA Puglia, which is the regional office in charge of the meteorological monitoring activities based on Meteorological Monitoring Systems. In this case, the weather station used as a reference to obtain climate data is located in the middle of the chosen area [22], and the initial settings for the microclimate simulations are reported in Tables 2 and 3.

**Table 2.** Initial settings for the microclimate simulation.

| Parameter | Value |
|---|---|
| Start date | July 21 |
| Total simulation time | 72 h |
| Wind speed | 3.4 m/s |
| Wind direction | 269° |
| Roughness length | 0.01 |
| Initial air temperature | 27.0 °C |
| Initial relative humidity | 29.9% |

**Table 3.** Air temperature and humidity values set in ENVI-met.

| | 12:00 a.m. | 01:00 a.m. | 02:00 a.m. | 03:00 a.m. | 04:00 a.m. | 05:00 a.m. | 06:00 a.m. | 07:00 a.m. | 08:00 a.m. | 09:00 a.m. | 10:00 a.m. | 11:00 a.m. |
|---|---|---|---|---|---|---|---|---|---|---|---|---|
| $T_{air}$ (°C) | 27.0 | 26.2 | 26.0 | 25.5 | 25.5 | 25.1 | 24.8 | 25.8 | 27.8 | 30.0 | 30.8 | 31.5 |
| RH (%) | 29.9 | 31.8 | 31.7 | 32.1 | 33.7 | 37.0 | 43.3 | 45.5 | 43.5 | 43.1 | 48.3 | 49.3 |
| | 12:00 p.m. | 01:00 p.m. | 02:00 p.m. | 03:00 p.m. | 04:00 p.m. | 05:00 p.m. | 06:00 p.m. | 07:00 p.m. | 08:00 p.m. | 09:00 p.m. | 10:00 p.m. | 11:00 p.m. |
| $T_{air}$ (°C) | 30.1 | 29.7 | 29.6 | 29.3 | 29.1 | 29.7 | 32.8 | 33.7 | 32.2 | 31.0 | 30.1 | 29.5 |
| RH (%) | 56.9 | 54.6 | 53.1 | 57.3 | 53.3 | 50.2 | 32.6 | 25.8 | 27.1 | 32.7 | 39.2 | 43.2 |

The simulation model's starting date was set as the 21st of July, chosen as the representative summer day based on real temperature data recorded; during this day, the highest summertime peak temperature was recorded (maximum daily air temperature of 33.7 °C at 07:00 p.m.). Moreover, an average difference between urban and rural areas of 4.8 °C was recorded, while the maximum intensity of the UHI during the day was reached at 12:00 a.m. and 5:00 a.m., with a value of 7.5 °C. Finally, the minimum UHI effect was reached at 08:00 a.m. with a value of 2.0 °C (Figure 4).
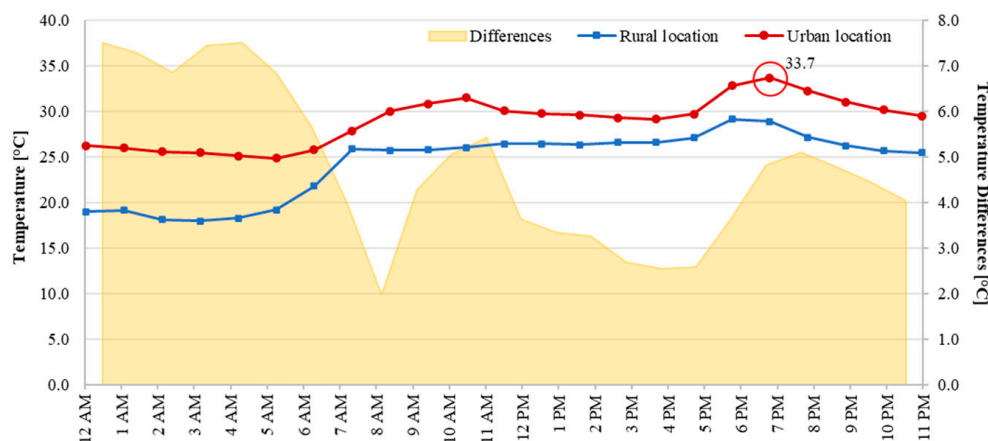


**Figure 4.** Daily air temperatures and daily differences in urban and rural locations (21st of July). The red circle represents the maximum air temperature.

The minimum simulation time suggested in the ENVI-met guide is 6 h [52]. Some authors considered less than 24 h of simulation, i.e., 6 h [53] or 15 h [54], and many authors considered 24 h of simulation [55,56]. Long-time simulation involves 45/48 h [57,58] or 72 h [59]; only a few times more than 3 days (5 days) [60] are simulated. To improve the reliability of the results, the simulation run time adopted in this study is three days (72 h). Three days is a reasonable compromise between accuracy and calculation time. The first 48 h of the model run—even if 24 h would be sufficient—is discarded due to the ENVI-met model's spin-up time requirement. While tripling the model-run time, this approach significantly increases the model's overall performance.

Hence, all simulations start at 12:00 a.m. on the 21st of July and end at 11:59 p.m. on the 23rd of July. The last day was considered the most reliable thanks to the higher model stability—reached within the first 48 simulation hours—and therefore was considered to draw the conclusions.

### 2.3. Mitigation Scenarios

In order to test the potential of different strategies, four different mitigated configurations of the model were developed; hence, including the baseline scenario, the following five scenarios were modeled and analyzed:

- Scenario 0—Baseline: The baseline scenario; the model represents the actual configuration of the considered area, and standard values of the urban environment—reported in Table 1—were applied.
- Scenario 1—Green roofs: Green roofs were applied to all buildings. Radiative properties of the building wall, pavements, and roads were the same as the baseline scenario, while roof grass albedo was 0.2 (Table 4).
- Scenario 2—Green walls: Green walls were applied to all buildings. Radiative properties of building roof, pavements, and streets were the same as the baseline scenario, while wall grass albedo was 0.2 (Table 4).
- Scenario 3—Cool roofs: All the roofs were assumed to be covered with high-reflectance material (albedo = 0.69, Table 4). Radiative properties of building walls, pavements, and roads were the same of the baseline scenario.
- Scenario 4—Cool walls: All the walls were assumed to be covered with high-reflectance material (albedo = 0.69, Table 4). Radiative properties of building walls, pavements, and roads were the same of the baseline scenario.

**Table 4.** Physical characteristics of new materials adopted for the mitigated scenarios.

| Element | Material | Roughness Length | Albedo | Emissivity |
|---|---|---|---|---|
| Green roof | Greening (last layer) | - | 0.2 | - |
| Green wall | Greening (last layer) | - | 0.2 | - |
| Cool roof | Cool material (last layer) | 0.01 | 0.69 | 0.9 |
| Cool wall | Cool material (last layer) | 0.01 | 0.69 | 0.9 |

Green technologies were chosen from those already available in the ENVI-met database without any further change while, with reference to cool materials, only the albedo was changed, setting it uniformly at 0.69 (Table 4). The albedo value did not exceed 0.7 because this value is considered to be the maximum potential, and for many materials, this might be hindered by ageing [61] with phenomena that can substantially reduce the mitigation potential as much as 50% [62]. Moreover, pavements and streets with solar reflectance (SR) values that are too high are more critical as they might cause glare.

### 2.4. Building Energy Modeling

As already mentioned, there is a strong correlation between urban heat island and building thermal energy performance. Hence, after the microclimate analyses, the same scenarios were analyzed from a building point of view in EnergyPlus to evaluate the energy-savings related to the microclimatic changes. EnergyPlus is an open-source software for building energy simulations in dynamic conditions that simulates the thermal and energy processes that characterize the building (heating/cooling, lighting, occupancy, etc.).

The effects of the mitigation strategies were tested on a representative reference residential building—the midrise apartment (Figure 5)—provided by the Department of Energy (DOE). The reference building is composed of 4 levels above ground, each one consisting of eight main thermal zones and one corridor. The building has a rectangular base of 46.33 m × 16.91 m; each apartment has 88.33 m, with a total area of each floor of 783.64 m$^2$, including the corridors.
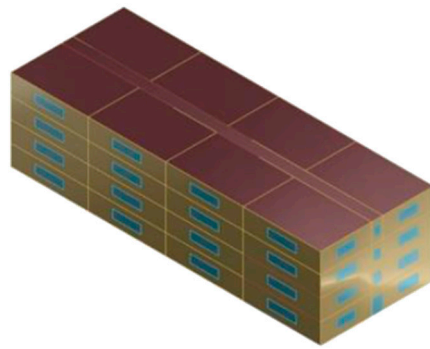
**Figure 5.** Geometrical characteristics of the midrise apartment reference building.

The analysis of the urban microclimate through ENVI-met allowed us to morph the climate data, obtaining new weather files—one for each simulated scenario—required to model the energy behavior of buildings. In particular, the new weather files were obtained by replacing the typical weather data with those obtained in the ENVI-met simulations. From an envelope point of view, the thermal and solar properties of the building were defined according to those imposed by the Italian law (Ministerial Decree 2015 [63]) as reported in Table 5.

**Table 5.** Envelope properties adopted for the building simulations.

| Building Components | Thermal Transmittance [W/m$^2$K] | Solar Heat Gain Coefficient [-] |
|---|---|---|
| Opaque walls | 0.34 | - |
| Opaque roofs | 0.33 | - |
| Slab | 0.38 | - |
| Windows | 2.2 | 0.35 |

Starting from these properties—adopted for Scenario 0—the building models of the mitigated scenarios were modified by applying the specific mitigation technology to the outer layer of the building envelope (green roof for Scenario 1, green wall for Scenario 2, cool roof for Scenario 3, and cool wall for Scenario 4). Hence, five different models (one reference and four mitigated scenarios) were set for the comparative energy analyses. Along with the characteristics of the envelope components, further important inputs were specified for evaluating the energy behavior of the building. An average occupancy of 2.5 people was assumed in the apartments and 2 people in the office area. From an artificial lighting point of view, the following power densities were assumed: 10.76 W/m$^2$ for the office area, 5.38 W/m$^2$ for the corridor, and 3.88 W/m$^2$ for the apartment; moreover, 12.9 W/m$^2$ and 5.38 W/m$^2$ were adopted as electrical equipment power density for the office area and apartment, respectively. Considering the green roof, a smart schedule was set, i.e., the program was forced by entering an irrigation schedule—regardless of the current soil moisture status—with a saturation limit for irrigation shutdown set to 70%. Considering the building systems, since the analysis was performed in the summertime, a 12 h period operation schedule of the cooling system was considered, from 10:00 a.m. to 10:00 p.m. Finally, the simulation period was set, according to the ENVI-met analyses, from the 21st to the 23rd of July, for a total of 72 h; however, the results obtained during the last day were considered the most reliable thanks to the model warm up that allows us to consider the transient nature of thermal phenomena.

## 3. Urban Heat Island Analysis: Results

The first analysis was performed considering the results of air temperature and surface temperature, paying attention to the variations related to the areas where mitigation technologies were implemented. Firstly, thermal maps of the selected area were simulated

by analyzing only Scenario 0 to define the initial configuration; then, this baseline was compared with the mitigated ones to highlight their differences. For all the scenarios, air temperature at 1.5 m was plotted to represent what people could perceive. For this part of the study, the results are all related to the last day of simulation (the 23rd of July) because this is the day when the highest temperatures occur, and the one that is less influenced by the model's initial instability. To define the benefits of a mitigation strategy, the following sections report the differences between the baseline temperatures (Scenario 0) and the analyzed mitigation scenarios. Consequently, absolute differences with negative values indicate that Scenario 0 is "cooler", whereas a positive value suggests it is "warmer" than the mitigated one. Moreover, to properly describe the thermal phenomena, the thermal maps are reported, considering three representative hours of the day: 7:00 a.m., 12:00 p.m., and 4:00 p.m.

The second analysis (Section 3.3) exclusively focuses on average air temperatures (derived from thermal maps), not considering the values referred to each pixel but their mean, obtaining hourly values plotted for the whole simulation period (21st–23rd of July). However, also in this case, only the last day was considered the most reliable of the whole period. For this second analysis, line charts were used to allow for a quantitative global reading and analysis of the behavior of each model. The following subsections describe in detail the outcomes of the simulations while the overall interpretation of results is reported in Sections 5 and 6.

### 3.1. Thermal Maps: Scenario 0 (Baseline)

Starting from the baseline scenario (Scenario 0, Figure 6), from 01:00 a.m. until 06:00 a.m., the air temperatures do not exceed 28.0 °C in the early hours of the day and do not drop below 25.0 °C. Albeit with a minimum difference, the area with higher temperatures is the main street of Corso Cavour and the secondary roads on the eastern side. Between 7 a.m. and 9 a.m., the maximum temperatures gradually rise up to 30.6 °C at 09:00 a.m. (26.9 °C at 07:00 a.m., 28.8 °C at 08:00 a.m.) while minimum temperatures reach 29.4 °C (26.2 °C at 07:00 a.m., 27.9 °C at 08:00 a.m.). During these first hours of the morning, the main road is characterized by inhomogeneous air temperatures due to the shading of the buildings. In the following hours, the maximum temperatures continue to rise rapidly reaching 31.7 °C at 10:00 a.m. up to a maximum temperature of 32.9 °C at 02:00 p.m. while the minimum temperature reaches 31.3 °C at 2:00 p.m. These temperatures are nearly steady during the following hours when the minimum temperature drops by 0.1 °C/0.2 °C, while the maximum temperature reaches 32.8 °C. Between 04:00 p.m. and 05:00 p.m., compared to the temperatures of the previous hour, there is a drop of about 0.5 °C for the whole scenario. Then, starting from 06:00 p.m., temperatures start to increase again, reaching 32.9 °C at 07:00 p.m.

At 08:00 p.m., the temperatures drop by about 1.0 °C with a maximum temperature ($T_{max}$) of 31.9 °C. A further drop in temperature is recorded at 09:00 p.m. with a minimum temperature ($T_{min}$) of 30.4 °C and a $T_{max}$ = 30.8 °C, at 10:00 p.m. ($T_{min}$ = 29.6 °C and $T_{max}$ = 30.2 °C) and at 11:00 p.m. ($T_{min}$ = 29.0 °C and $T_{max}$ = 29.7 °C).

Considering the surface temperatures (Figure 7), from 01:00 a.m. to 05:00 a.m., the scenario is characterized by an average surface temperature between 27.0 °C and 29.0 °C on both secondary and main roads. At 07:00 a.m., for the secondary roads in the East–West direction, the temperatures range between 29.7 °C and 33.9 °C, while in all the others, they are between 26.9 °C and 28.3 °C because of the direct solar radiation. In the following hours, temperatures rise, and at 10:00 a.m., along the main road, the highest temperatures are recorded in the asphalted areas (between 41.1 °C and 50.3 °C) while the lowest temperatures are registered in the tree-lined areas (between 29.0 °C and 32.0 °C). Similarly, at 12:00 p.m., along the main road, the highest temperatures are recorded in the asphalted areas (between 48.2 °C and 55.3 °C) while the lowest temperatures in the tree-lined areas range between 30.5 °C and 34.0 °C. The surface temperatures continue to rise, reaching its maximum at 01:00 p.m. (56.0 °C). Then, the temperatures start to drop: at 04:00 p.m., the temperatures of

the secondary roads in the East–West direction oscillate between 41.3 °C and 50.5 °C, while in the North–South direction, they do not exceed 38.2 °C. In the late afternoon (06:00 p.m.), except for the tree-lined areas where temperatures range between 31.4 °C and 33.4 °C, the scenario average temperature is about 36.0 °C and further drops to 34.0 °C at 07:00 p.m. and to 30.0 °C at 11:00 p.m.
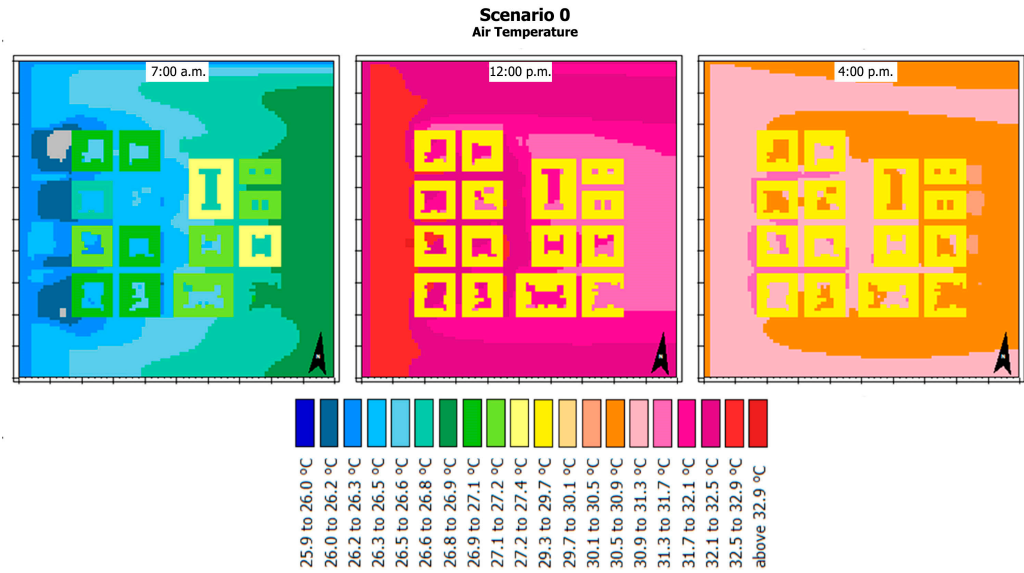


**Figure 6.** Scenario 0: Air temperatures during three representative hours registered on the 23rd of July: 7:00 a.m. (**left**), 12:00 p.m. (**middle**), and 4:00 p.m. (**right**).
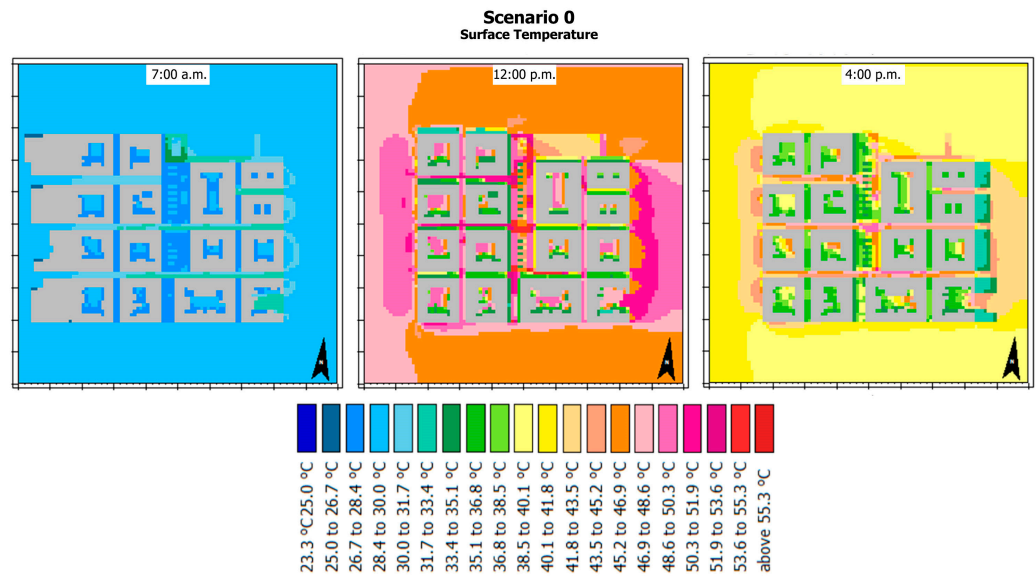


**Figure 7.** Scenario 0: Surface temperatures during three representative hours registered on the 23rd of July: 7:00 a.m. (**left**), 12:00 p.m. (**middle**), and 4:00 p.m. (**right**).

### 3.2. Thermal Maps: Mitigation Scenarios

The results obtained from the simulations are presented in the pictures below (Figures 8 and 9), scenario by scenario, and are discussed in the following subsections, comparing them with Scenario 0 with a specific focus on air temperature and surface temperature. The results are discussed as temperature differences between baseline and the mitigated model; it follows that negative differences represent a baseline cooler than the mitigated model and vice versa when the differences are positive.
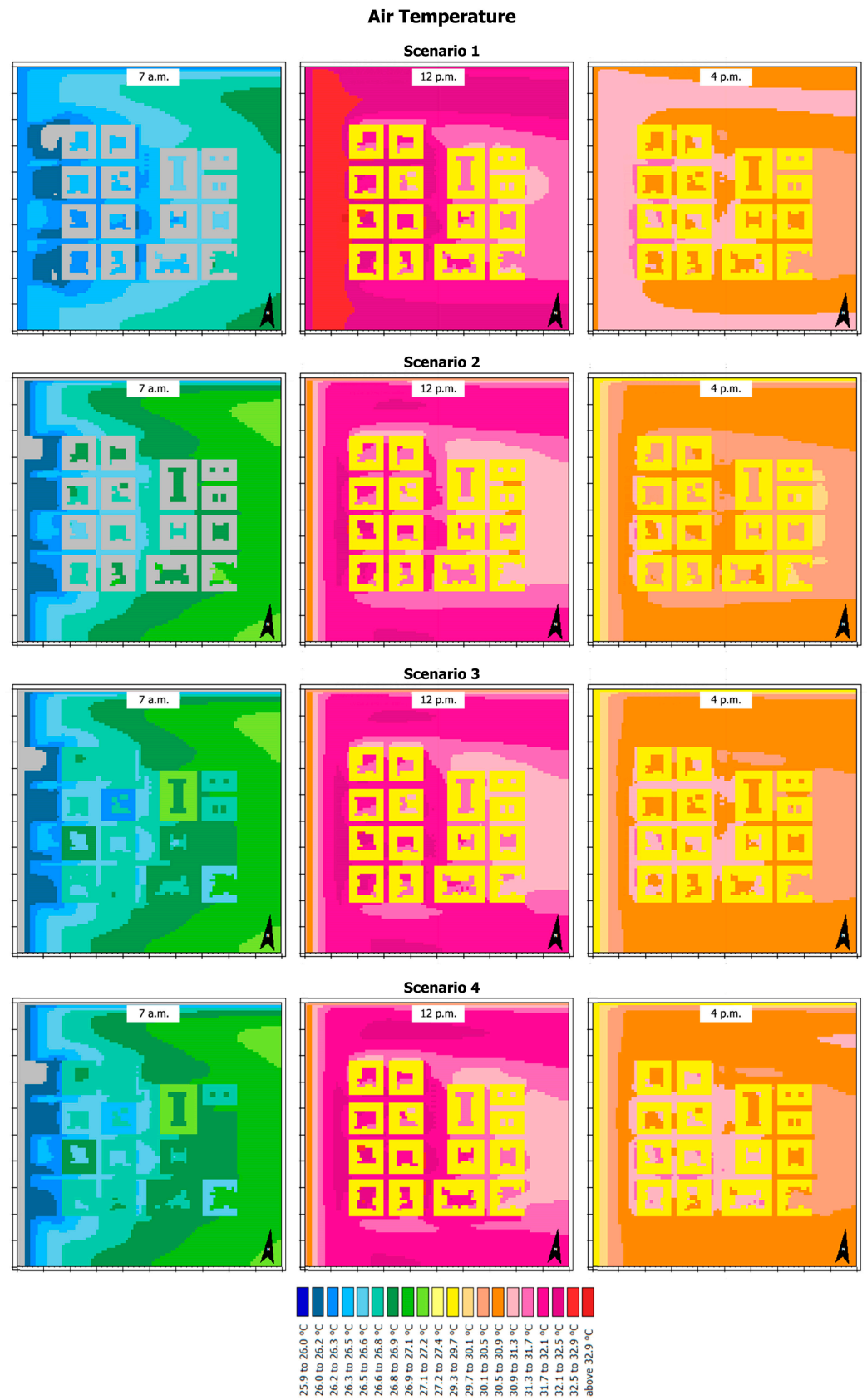
**Figure 8.** Thermal maps of air temperatures for Scenarios 1–4, registered on the 23rd of July.
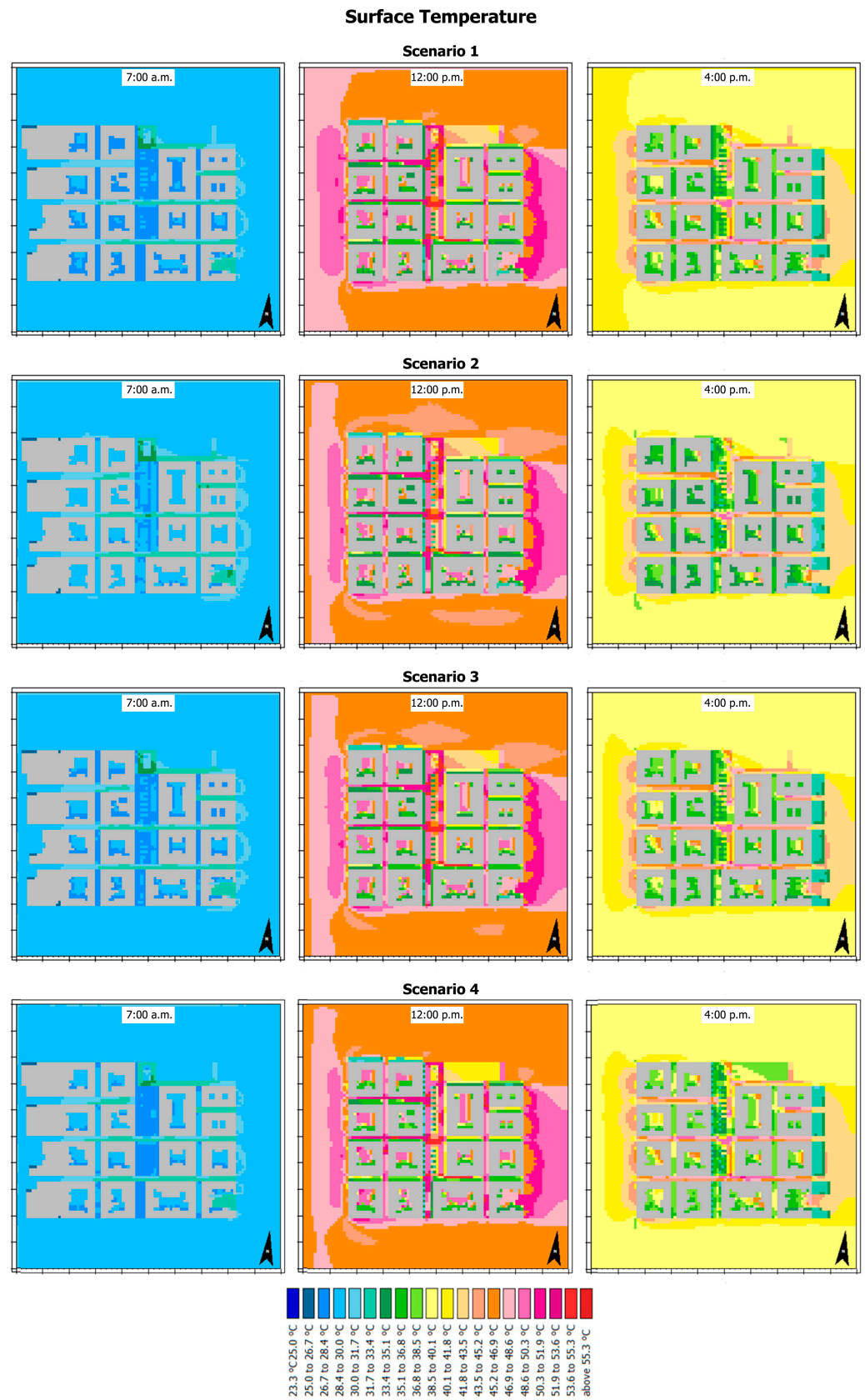
**Surface Temperature**



**Figure 9.** Thermal maps of surface temperatures for Scenarios 1–4, registered on the 23rd of July.

3.2.1. Scenario 1: Green Roofs

From an air temperature point of view, the two scenarios exhibit the same temperatures from 12:00 a.m. to 05:00 a.m. At 06:00 a.m., slight differences (nearly 0.1 °C) can be registered only in the eastern part of the model and in the southern part of the main road. At 07:00 a.m., these differences begin to extend towards the west side of the model and reach a maximum of 0.2 °C in some points of the eastern secondary roads. From 07:00 a.m. to 11:00 a.m., the differences in temperature are still between 0.1 °C and 0.2 °C, with slight differences only in their pattern throughout the model. Similar trends are reported from 12:00 a.m. until 05:00 p.m. when larger differences (0.3 °C in the eastern secondary roads) are recorded. Then, the differences start to decrease, ranging between 0 °C and 0.1 °C, at 07:00 p.m. and become completely negligible after 10:00 p.m.

Considering the surface temperature, from 12:00 a.m. to 06:00 a.m., only limited differences (0.1 °C) can be identified in the eastern part of the model. From 07:00 a.m. onwards, the whole scenario presents larger differences (between −0.3 °C and 0.3 °C). At 12:00 p.m., the roads on the eastern side of the model show a temperature difference between 0.1 °C and 0.3 °C, which also extends along the main road in the following hours, while in the remaining streets, it is between −0.4 °C and 0.1 °C. In the afternoon—until 06:00 p.m.—sensible differences (between 0.1 °C and 0.3 °C) are still registered, while these differences drop to 0.1 °C between 07:00 p.m. and 08:00 p.m. and are negligible in the following hours.

3.2.2. Scenario 2: Green Walls

Considering the air temperature, during the first hours of the simulations (12:00 a.m.–05:00 a.m.), Scenario 0 is cooler than Scenario 2, with differences that range mainly between −0.5 °C and −0.1 °C, with a maximum difference (−0.7 °C) registered for the main road, in particular on the western sidewalks. These differences gradually decrease (−0.2 °C and 0.0 °C at 07:00 a.m.), reversing their trend at 08:00 a.m. (between −0.2 °C and +0.3 °C). From 09:00 a.m. onwards, the mitigated scenario is always cooler than the baseline (between 0.1 °C and 0.3 °C). After 10:00 a.m., the benefits of the mitigation strategy are clearer, reaching differences ranging between 0.4 °C and 1.0 °C. This trend is also confirmed in the following hours, until 02:00 p.m., when the differences are slightly lower (between 0.2 °C and 0.8 °C). Similar values are registered in the early afternoon until 05:00 p.m. when most of the secondary roads show a difference between 0.4 °C and 0.9 °C, while the remaining areas of the model range between 0.2 °C and 0.8 °C. Later (06:00–07:00 p.m.), the models show mostly differences between 0.7 °C and 0.9 °C and start to reduce their divergence from 08:00 p.m. onwards. At 09:00 p.m., the differences are already lower than 0.5 °C and become negligible after 10:00 p.m.

Considering the surface temperature, also in this case, the baseline scenario is cooler during the night, until 08:00–09:00 a.m. when differences between −0.5 °C and +0.5 °C are registered. During the morning, the mitigation strategy shows its benefits—until 12:00 a.m.— reducing the surface temperatures by nearly 0.5 °C, except for the central tree-lined area of the main road, where lower benefits are shown. These differences increase during the afternoon (between 0.3 °C and 1.3 °C at 04:00 p.m.) reaching their maximum at 06:00 p.m. when differences between 1.4 °C and 1.7 °C are registered for the secondary roads, and between 0.6 °C and 1.1 °C for the main one. The differences drop in the following hours, and at 09:00 p.m., they become negative in the whole model except for the main road (between 0.1 °C and 0.3 °C).

3.2.3. Scenario 3: Cool Roofs

Considering the variation of the air temperatures, between 12:00 a.m. and 06:00 a.m., the baseline scenario is cooler than the mitigated scenario with differences that range between −0.5 °C and −0.2 °C. These differences are smaller at 07:00 a.m. (between −0.3 °C and −0.1 °C) and the trend is reversed at 08:00 a.m. when a difference between 0.0 °C and 0.1 °C is present almost uniformly throughout the model. During the morning, the

divergences of the two models become more noticeable, reaching a maximum difference of 0.4 °C at 11:00 a.m.; these values are quite stable up to 04:00 p.m. when a nearly uniform difference of 0.2 °C is registered in the whole area. Then, the differences rise up to 0.6 °C at 07:00 p.m. and begin to drop after 08:00 p.m. when the differences range between 0.3 °C and 0.5 °C. At 09:00 p.m., the differences are already nearly negligible (between 0.1 °C and 0.3 °C) and become less evident at 11:00 p.m. (lower than 0.2 °C).

Moving to the surface temperature, the two scenarios show similar values fluctuating between −0.3 °C and +0.2 °C during the night, with the highest values registered in relation to the main road. Then, during the day, at 12:00 p.m., the two models show differences that range from −0.9 °C to 0.2 °C, dropping between −0.5 °C and 0.2 °C at 04:00 p.m. On the contrary, at 05:00 p.m., differences between −0.1 °C and 0.2 °C are registered, while at 08:00 p.m., these values fluctuate between 0.1 °C and 0.4 °C and remain almost unvaried until 11:00 p.m.

### 3.2.4. Scenario 4: Cool Walls

Starting from the air temperature, from 12:00 a.m. to 06:00 a.m., the baseline scenario is cooler than the mitigated scenario with differences that range from −0.4 °C to −0.1 °C, with the highest differences registered for the main road and between 03:00 a.m. and 06:00 a.m. These differences are limited at 07:00 a.m. (around −0.1 °C) and the trend is reversed from 08:00 a.m. onwards when the differences fluctuate around 0 °C and 0.1 °C. The divergence of the two models increases in the following hours, reaching its peak at 11:00 a.m. when the mitigated scenario is significantly cooler compared to the baseline (between 0.3 °C and 0.4 °C). In the following hours, the differences are slightly lower, fluctuating around 0.1 °C and 0.3 °C, between 12:00 a.m. and 03:00 p.m. A further decrease is recorded at 04:00 p.m. (0.1 °C) when the two models start to show larger variations, peaking at 07:00 p.m., with differences that range from 0.4 °C and 0.6 °C. In the following hours, the two models gradually converge towards similar temperatures (differences between 0.3 °C and 0.5 °C at 08:00 p.m., 0.1 °C and 0.3 °C at 09:00 p.m., and around 0.1 °C between 10:00 p.m. and 11:00 p.m.).

With reference to the surface temperature, during the night—from 12:00 a.m. to 06:00 a.m.—the two models significantly differ with regard to the roads (differences between −0.2 °C and +0.3 °C) and the paved areas where the mitigated scenario is significantly cooler than the baseline (up to 1.5 °C cooler). At 07:00 a.m., secondary roads have lower temperatures in the baseline scenario, with differences between −0.7 °C and −0.1 °C, while along the main road, they range between −0.1 °C and 0.6 °C, exceeding 0.6 °C (up to 0.9 °C) in a few areas close to the western sidewalks. These differences increase within the following hours in the following manner: negatively along the secondary roads and positively along the main one. Indeed, at 12:00 p.m., the temperature differences along the secondary roads range between −1.0 °C and 0.1 °C. On the contrary, along the main road, there is a difference between 0.1 °C and 1.2 °C in the asphalted areas, while at the sidewalks, the differences range between 1.2 °C and 2.3 °C. A similar trend is observed in the following hours, with negative differences for the secondary roads and positive for the main one. At 04:00 p.m., the secondary roads register differences between −0.7 °C and 0.1 °C, while along the main road, the differences fluctuate between −0.5 °C and 1.4 °C in the asphalted areas and between 0.7 °C, up to 2.7 °C in the paved areas. In the following hours, until 11:00 pm, the differences along the secondary roads remain negative but reduced in magnitude; along the sidewalks, the differences decrease between 1.0 °C and 2.0 °C while the asphalted areas record a difference between 0.4 °C and 0.7 °C.

### 3.3. Overall Urban Heat Island Comparisons

To better understand how the application of the different mitigation strategies contributes to the reduction in the UHI phenomenon, hourly data were collected from each simulation and compared. These data were obtained by averaging the temperature values of each pixel of the analysis grid of thermal maps, for each hour and for each simulated

scenario. Figure 10 shows the hourly air temperature values of all the scenarios during the three simulation days and the typical weather file represented with the dotted line. However, as already mentioned, only the last day was considered in the discussion as it is considered the most reliable thanks to the higher model stability. The main effects of the UHI phenomenon clearly emerge from a comparison between the standard values (dotted line) and the baseline (Scenario 0, blue line). Especially between 06:00 p.m. and 08:00 a.m., the reference temperatures have significantly lower values with hourly differences up to 6.0 °C, and an average daily difference of about 2.2 °C.
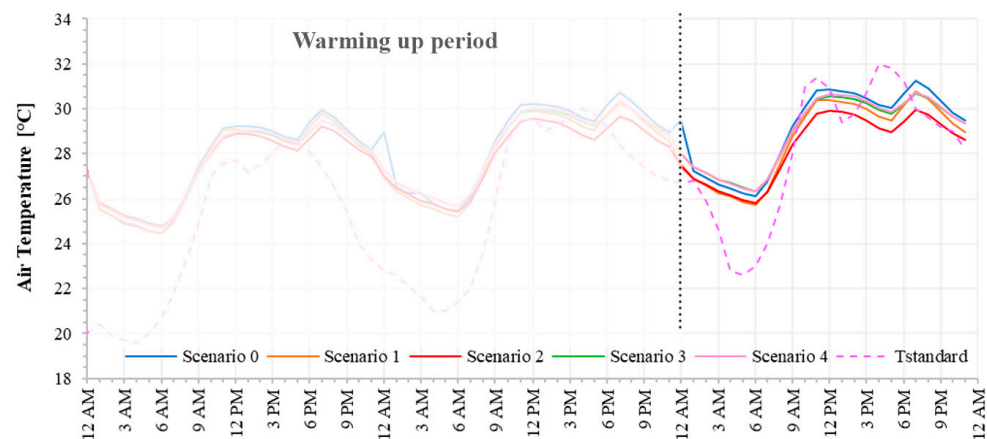


**Figure 10.** Hourly air temperature during three representative days for all scenarios (continuous lines) and typical weather file (dotted line).

During the three simulated days, the temperatures increase. At the beginning of the simulation (21st of July), no scenario exceeds 30.0 °C, while all scenarios reach the highest temperature at 07:00 p.m. on the 23rd of July (31.2 °C for Scenario 0, 30.8 °C for Scenario 1, 30.0 °C for Scenario 2, and 30.7 °C for Scenario 3 and Scenario 4). In general, Scenario 0 shows the highest temperatures. Between 06:00 a.m. and 09:00 a.m. the temperatures of all the scenarios tend to be similar. However, during these hours, Scenario 0 generally remains the hottest, followed by Scenarios 3 and 4, Scenario 1, and Scenario 2. In the remaining hours, the difference between the scenarios becomes clearer. Between 11:00 a.m. and 01:00 p.m., Scenario 0 remains the hottest, followed by Scenario 4, Scenario 3, Scenario 1, and Scenario 2 that record temperatures up to 1.0 °C lower than Scenario 0.

A more detailed analysis of the differences between Scenario 0 and each mitigation scenarios was conducted. As already mentioned, negative differences indicate that Scenario 0 has lower temperatures than the mitigation scenario considered; conversely, positive values of the differences indicate that the mitigation scenario has lower temperatures than Scenario 0. By comparing Scenario 0 and Scenario 1 (green roofs), a rising trend in the air temperature differences can be deducted (Figure 11). At the beginning of the simulation, no differences can be identified between the two models while—as the model steadies—the different behaviors between the scenarios emerge. Indeed, on the 23rd of July, there was a difference of 0.4 °C from the beginning of the day until 12:00 p.m. and it gradually reached 0.5 °C at 06:00 p.m. and fluctuated around 0.5 °C until the end of the simulation. Therefore, overall, the implementation of green roofs leads to lower temperatures compared with Scenario 0, with significant peaks between 12:00 a.m. and 06:00 p.m.
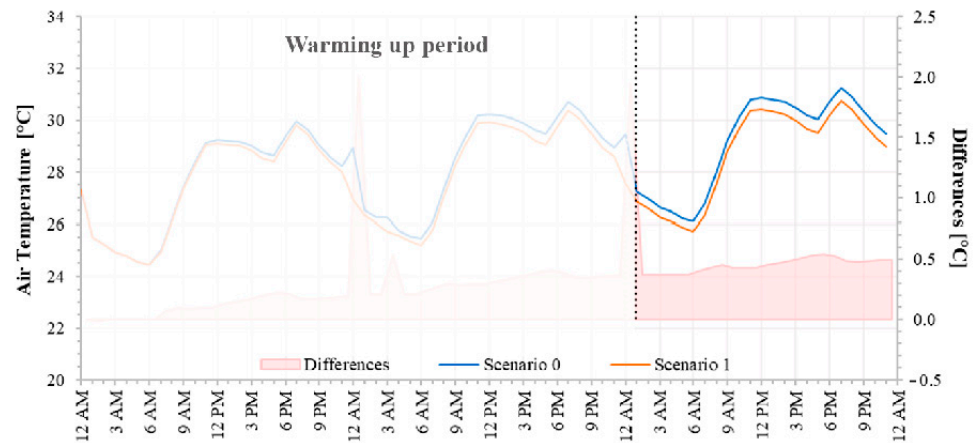
**Figure 11.** Hourly air temperature and differences between Scenario 0 and Scenario 1.

By comparing Scenario 0 and Scenario 2 (green walls), the temperature differences are larger than in the previous comparison, and variability is also greater as shown in Figure 12. As already mentioned in the previous scenario, the differences between the two models mainly emerge during the last day. In the first hours of the of the 23rd of July, the differences hover around 0.3 °C, with a slightly decreasing trend, and become more evident from 07:00 a.m. onwards. Indeed, the differences gradually increase from 0.3 °C, reaching 1.0 °C at 11:00 a.m. (until 04:00 p.m.); the benefits are maximized at 06:00 p.m. when the mitigated scenario is 1.3 °C cooler than the baseline and settles at 0.9 °C at 11:00 p.m. Also, in this case, the green walls scenario has lower temperatures than Scenario 0, with larger benefits compared to the previous analysis.
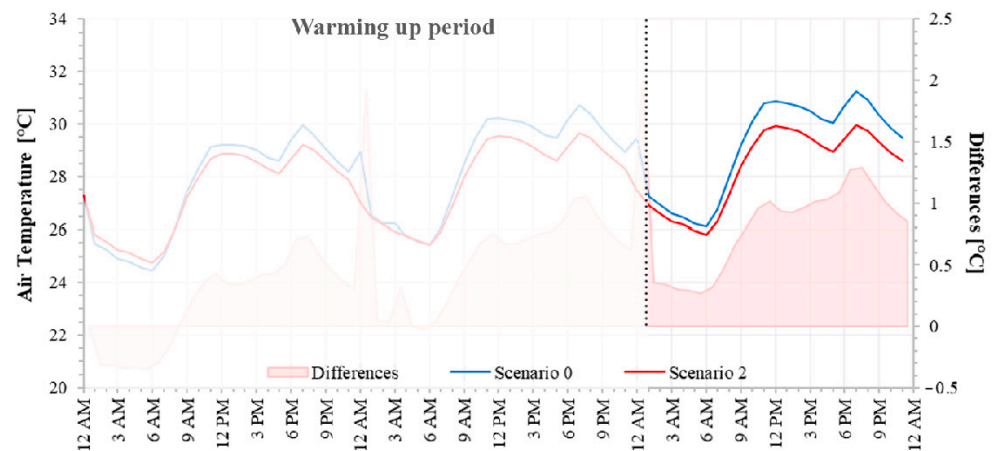


**Figure 12.** Hourly air temperature and differences between Scenario 0 and Scenario 2.

Scenario 3 (cool roofs) shows negative differences compared to Scenario 0 (between −0.3 °C and −0.1 °C) from 12:00 a.m. and 07:00 a.m., as shown in Figure 13. During the last day, differences between 0.1 °C and 0.4 °C are registered between 08:00 a.m. and 11:00 a.m., with an increase of 0.1 °C every hour; then, the differences settle at 0.2 °C until 05:00 p.m. During the evening, these differences peak at 0.5 °C at 07:00 p.m. and then drop to 0.1 °C at 11:00 p.m. Although to a lesser extent than the other mitigation scenarios, the implementation of cool roofs also records temperatures that are overall lower than Scenario 0.
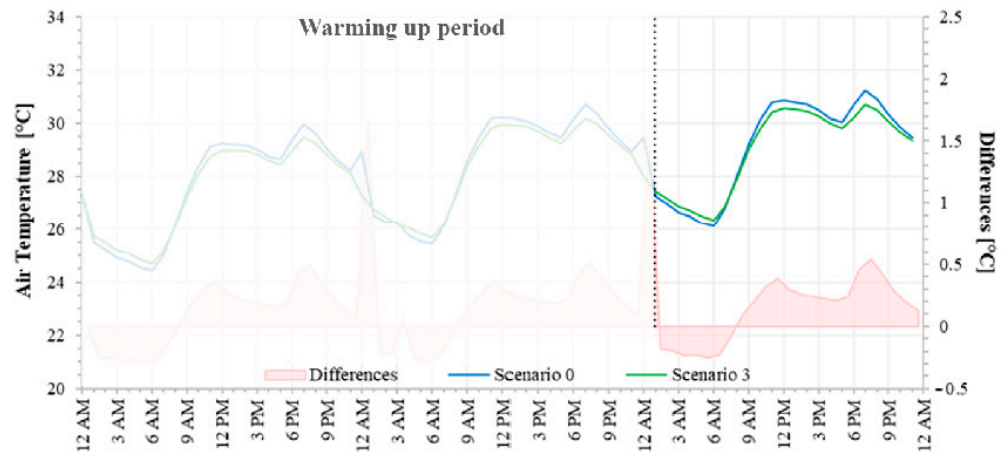
**Figure 13.** Hourly air temperature and differences between Scenario 0 and Scenario 3.

Scenario 4 (cool walls) shows a temperature trend very similar to Scenario 3 (Figure 14). Focusing on the 23rd of July, negative differences are registered from 12:00 a.m. and 07:00 a.m. (around −0.3 °C) while the mitigated scenario shows its benefits from 08:00 a.m. to 11:00 a.m. (differences between 0.1 °C and 0.3 °C), with an increase of 0.1 °C every hour. Then, the differences settle at 0.2 °C until 05:00 p.m., reach 0.5 °C at 07:00 p.m., and drop to 0.1 °C at 11:00 p.m. As for the other scenarios, temperatures for Scenario 4 are overall lower than Scenario 0.
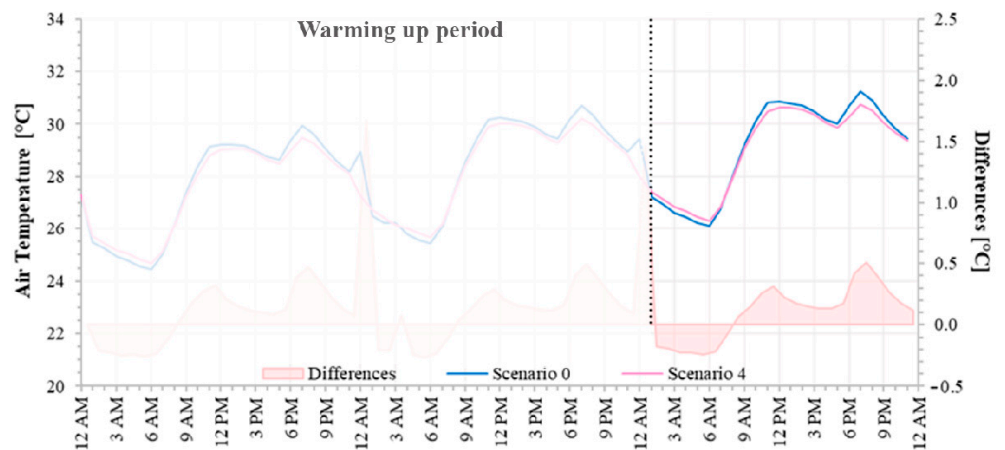


**Figure 14.** Hourly air temperature and differences between Scenario 0 and Scenario 4.

In general, as the stability of the model and the temperature of the scenarios increases, from the 21st to 23rd of July, the positive effects of the mitigation technologies grow, except for Scenario 3 and Scenario 4, where the three days show very similar trends. Following these analyses and looking at the average daily air temperatures (Table 6), Scenario 2 (green walls) has the greatest daily air temperature mitigation effects with a difference—compared to Scenario 0—of 0.8 °C on July 23. It is followed by Scenario 1 (green roofs), with a maximum daily difference of 0.5 °C, and Scenario 3 (cool roofs) and 4 (cool walls) with a maximum daily difference of 0.2 °C.

**Table 6.** Daily average and differences in air temperature for scenarios 0, 1, 2, 3, and 4.

| Day | Air Temperature [°C] | | | | | | | | |
|---|---|---|---|---|---|---|---|---|---|
| | Scenario 0 | Scenario 1 | Scenario 2 | Scenario 3 | Scenario 4 | 0–1 | 0–2 | 0–3 | 0–4 |
| 21-Jul | 27.6 | 27.5 (−0.4%) | 27.4 (−0.7%) | 27.5 (−0.4%) | 27.5 (−0.4%) | 0.1 | 0.2 | 0.1 | 0.1 |
| 22-Jul | 28.5 | 28.2 (−1.1%) | 27.9 (−2.1%) | 28.4 (−0.4%) | 28.4 (−0.4%) | 0.4 | 0.6 | 0.2 | 0.2 |
| 23-Jul | 29.1 | 28.6 (−1.7%) | 28.3 (−2.7%) | 29.0 (−0.3%) | 29.0 (−0.3%) | 0.5 | 0.8 | 0.2 | 0.2 |

## 4. Building Energy Analysis: Results

Since the analysis was carried out in the summer, only the energy consumption for cooling was considered. The energy data were analyzed as hourly, daily, and global consumption differences over the three days, by averaging the consumption, which was calculated firstly by exposure and then by considering all the thermal zones. Negative differences indicate that Scenario 0 has lower energy consumption than in the mitigation scenario; conversely, positive differences indicate that Scenario 0 shows higher energy consumption than the mitigation scenario.

### 4.1. North

Considering the northern exposure, the daily average of the difference in consumption (Figure 15a) shows that on the 23rd of July, Scenario 3 offers the highest savings (4.6%), and very similar values are registered for the cool walls modeled in Scenario 4 (4.5%). On the contrary, Scenario 2 essentially registers negligible differences when compared to the baseline while Scenario 1 shows an intermediate behavior (2.3%).
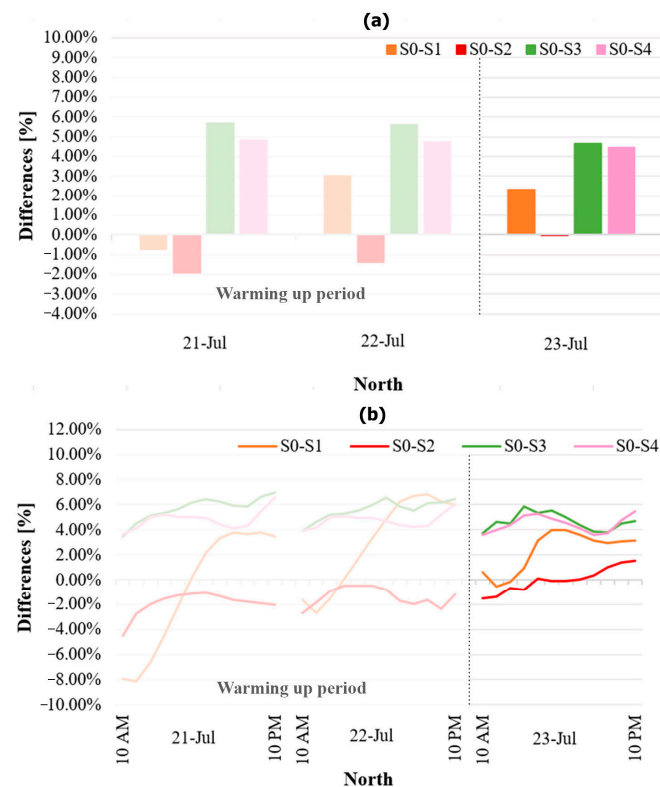


**Figure 15.** Daily average percentage differences (**a**) and hourly percentage differences (**b**) in cooling energy consumption for the northern exposures (S1, S3, and S4 perform better than S0, while S2 shows higher cooling energy consumption compared to S0).

Comparing hourly differences for the same exposure (Figure 15b) on the 23rd of July, the consumption of Scenario 0 is similar to Scenario 1, until the middle of the day. In the second half of the day, Scenario 1 records consumptions between 1.0% and 4.0% lower than Scenario 0. Instead, comparing Scenario 0 with Scenario 2, except for a few hours at the beginning of the day, Scenario 2 shows higher consumption: the differences between the two range between −2.0% and 0%. The comparison between Scenario 0 and scenarios 3 and 4 leads to completely different results. In general, the two mitigation scenarios show lower consumption than Scenario 0 during the whole day, with differences varying from 4.0% to 6.0% for Scenario 3 and from 4.0% to 5.0% for Scenario 4.

### 4.2. Northeast

Considering the northeastern exposure, the daily average difference in consumption (Figure 16a) shows a trend similar to the previous exposure. On the last day of the simulation, Scenario 1 allows us to reduce the energy consumption by nearly 3% while negligible differences (−0.16%) are recorded for Scenario 2. On the contrary, scenarios 3 and 4 show similar trends highlighting more noticeable benefits, thus reducing the consumption by nearly 4.5% and 5.5%, respectively, compared to the baseline.
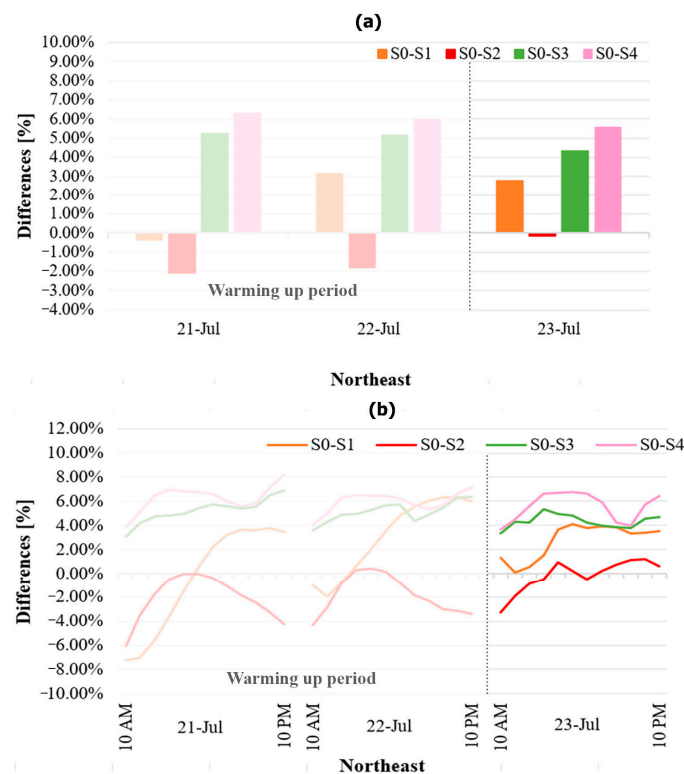


**Figure 16.** (**a**) Daily average percentage differences and (**b**) hourly percentage differences in cooling energy consumption for northeastern exposure (S1, S3, and S4 perform better than S0, while S2 shows higher cooling energy consumption compared to S0).

Considering the hourly averages (Figure 16b), during the first half of the 23rd of July, the highest consumption is recorded in Scenario 2, which registers differences between −4% and 0%, while in the second part of the day, benefits up to 1.5% are recorded. A similar rising trend characterizes Scenario 1, where the differences fluctuate between 0% (beginning of the day) and 4% in the second part of the day. Instead, for this exposure, Scenario 4 is the one with the lowest consumption, with differences that fluctuate between 4.0% and 7.0%, whereas for Scenario 3, differences range from 4.0% to 6.0%.

### 4.3. Northwest

Moving to the northwestern exposure, the daily differences (Figure 17a) on the 23rd of July range between 2% (Scenario 2) and 6% (Scenario 4) with intermediate differences recorded for Scenario 3 (4%) and Scenario 1 (2.5%). Therefore, all the analyzed technologies reduce energy consumption compared to the baseline.
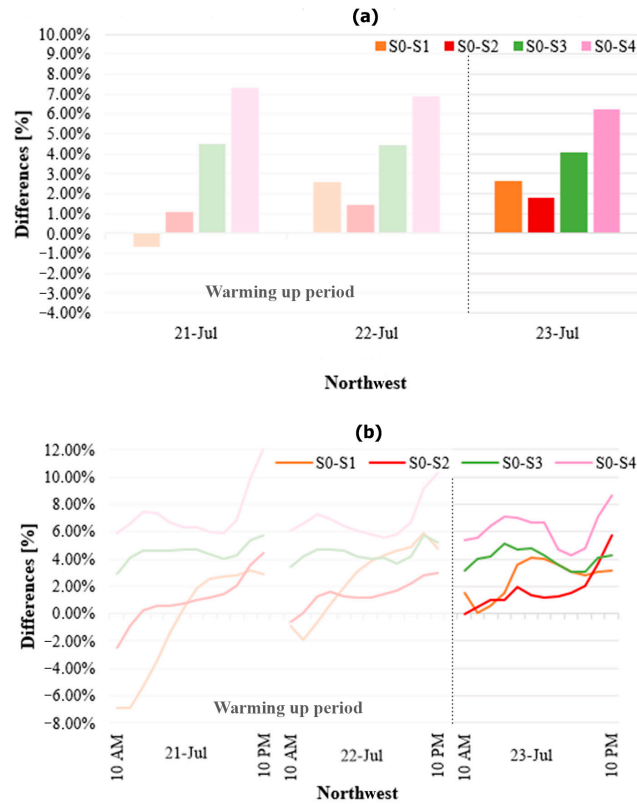


**Figure 17.** (**a**) Daily average percentage differences and (**b**) hourly percentage differences in cooling energy consumption for northwestern exposure (all scenarios performed better than S0).

Considering the hourly differences (Figure 17b), on the 23rd of July, all the scenarios show a positive difference throughout the whole day. Nevertheless, while scenarios 1 and 2 show a rising trend—ranging nearly between 0% and 4%—Scenarios 3 and 4 are characterized by higher and steadier benefits. Specifically, Scenario 3 shows differences ranging between 3.0% and 5.0%. For Scenario 4, consumption savings range from 5.0% to 7.0% in the first part of the day and from 4% and 8% in the second part of the day, peaking over 8.0% from 08:00 p.m. to 10:00 p.m.

### 4.4. South

Considering the daily average differences in consumption (Figure 18a) for the southern exposure, all the technologies considered shows beneficial effects compared to the baseline. The highest benefits (5%) are recorded in Scenario 4, followed by Scenario 3 (4.5%), Scenario 1 (2.2%), and Scenario 2 (1.0%). Concerning the hourly differences (Figure 18b) during the last simulated day, Scenario 1 shows consumption lower than Scenario 0, between 0% and 4.0%. The consumptions related to Scenario 2 are steady—around 2% lower than baseline—during the whole day except for the first hours (10:00 a.m.–12:00 p.m.) when the consumptions are higher in the mitigated scenario. On the contrary, Scenario 3 and Scenario 4 exhibit similar differences compared to Scenario 0, ranging from 4.0% during the earlier hours of the day, up to 6.0% in the afternoon; however, overall, the cool walls (Scenario 4) perform better than the cool roofs (Scenario 3) for the southern exposure.
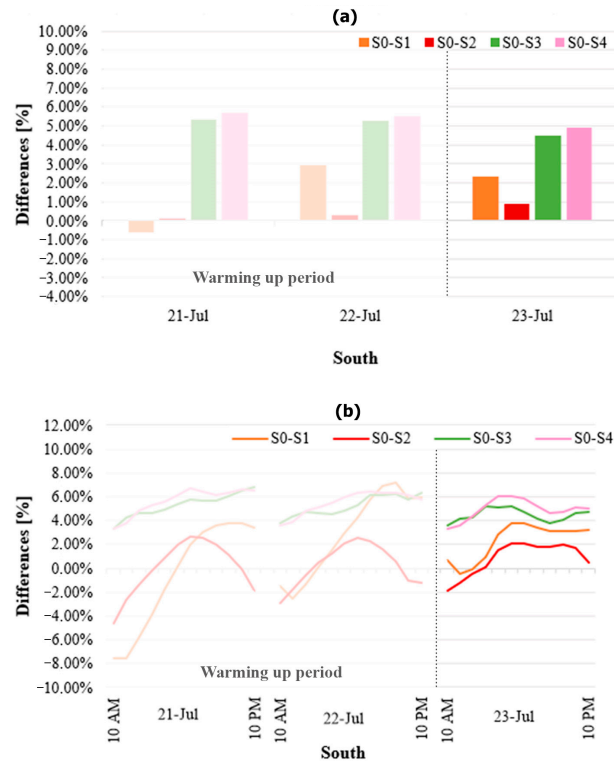
**Figure 18.** (**a**) Daily average percentage differences and (**b**) hourly percentage differences in cooling energy consumption for southern exposure (all scenarios performed better than S0, particularly S1, S3, and S4).

*4.5. Southeast*

Looking at the daily differences in consumption (Figure 19a), all the considered technologies improve the building energy performance. The lowest benefits are related to Scenario 2 (0.5%) while the differences are gradually higher for Scenario 1 (2.8%), Scenario 3 (4%), and Scenario 4 (5.5%).

Results similar to the previous exposure are obtained in hourly percentage differences for southeast-facing zones (Figure 19b). Scenario 1 exhibits more marked differences—compared to the previous exposure—saving over 4.0% on the 23rd of July. On the contrary, Scenario 0's consumption is lower than that of Scenario 2 during the first three hours; however, in the following hours, the savings deriving from applying the green facades are quite evident when the differences peak at 2.0% (at 07:00 p.m.) on the last day. Scenario 4 records a significant cooling saving compared to Scenario 0, reaching over 6.0% in the afternoon. Positive results are also registered for Scenario 3, with differences that range between 2.5% and 6.0% on the 23rd of July.
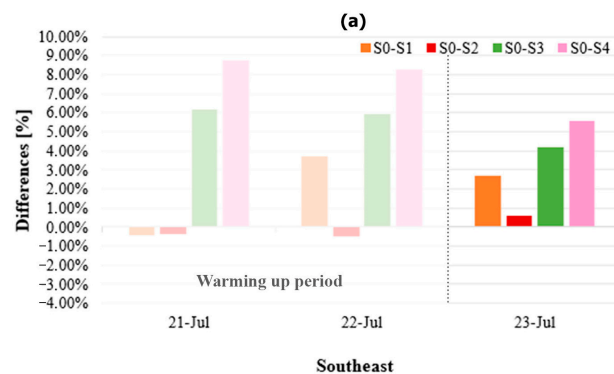


**Figure 19.** *Cont.*
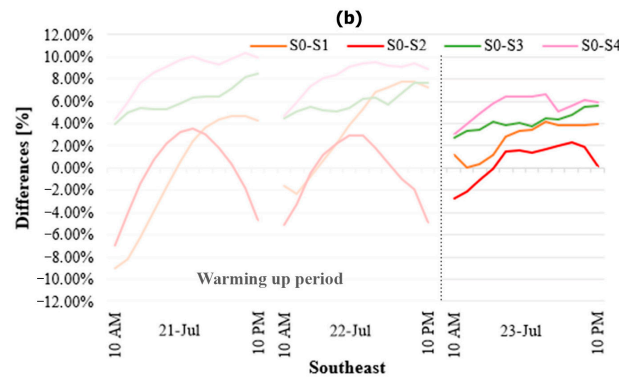
**Figure 19.** (**a**) Daily average percentage differences and (**b**) hourly percentage differences in cooling energy consumption for southeastern exposure (all scenarios perform better than S0, particularly S1, S3s and S4).

### 4.6. Southwest

With reference to scenarios 1 and 2, the daily average differences in consumption (Figure 20a) highlight good behavior (2.5% lower than the baseline) for both green roofs and walls (July 23). The benefits are higher for the cool technologies, as the cool roofs (Scenario 3) save 4% compared to the baseline, while the cool walls (Scenario 4) reach nearly 6.5%.
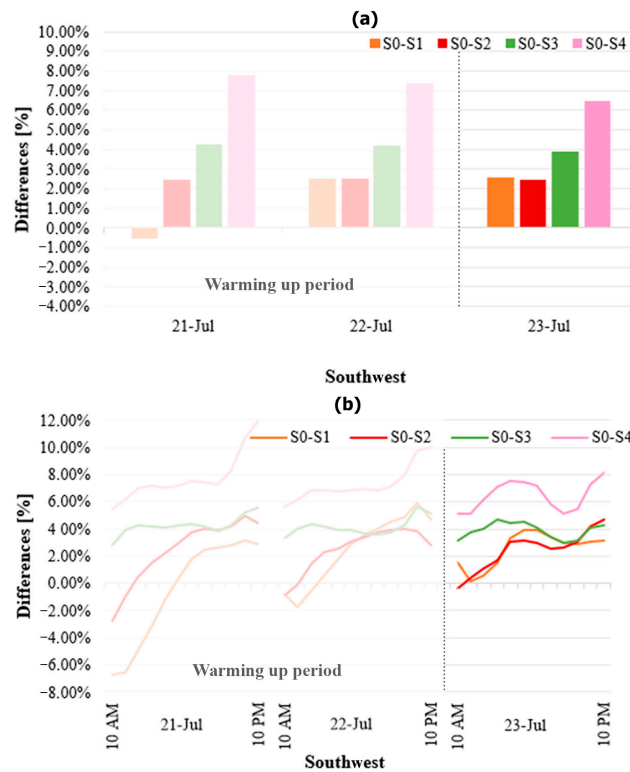


**Figure 20.** (**a**) Daily average percentage differences and (**b**) hourly percentage differences in cooling energy consumption for southwestern exposure (all scenarios perform better than S0, particularly S4).

Moving to the hourly differences (Figure 20b), all the technologies register a rising trend in the first hours of the day (July 23) and a more stable trend during the afternoon except for Scenario 4, which is more fluctuating. Scenarios 1 and 2 show similar trends ranging between 0—during the first hours—and nearly 4%, during the afternoon and evening, respectively. Scenario 3 still shows a slight variation, but it is limited to the 3–5%

range. The highest benefits are registered for the Scenario 4, which ranges between 5% and 8% during the during the day, reaching its maximum at 10:00 p.m.

### 4.7. Overall Results

To sum up the energy analyses conducted, Figure 21a shows the total consumption of every scenario represented as the sum of consumptions of all the exposures for each day, while Figure 21b shows the daily averages of the differences between each scenario and the baseline (Scenario 0). According to these results, Scenario 0 exhibits the highest consumption ($0.23$ kWh/m$^2$), while Scenario 4 exhibits the lowest one, reaching daily differences larger than 5.0% on the 23rd of July ($0.22$ kWh/m$^2$). On the same day, Scenario 3 shows an energy-saving rate of 4.0% ($0.22$ kWh/m$^2$) and Scenario 1 saves up to 2.2%. Instead, the lowest differences are related to Scenario 2, whose benefits are limited to 0.7% ($0.23$ kWh/m$^2$).
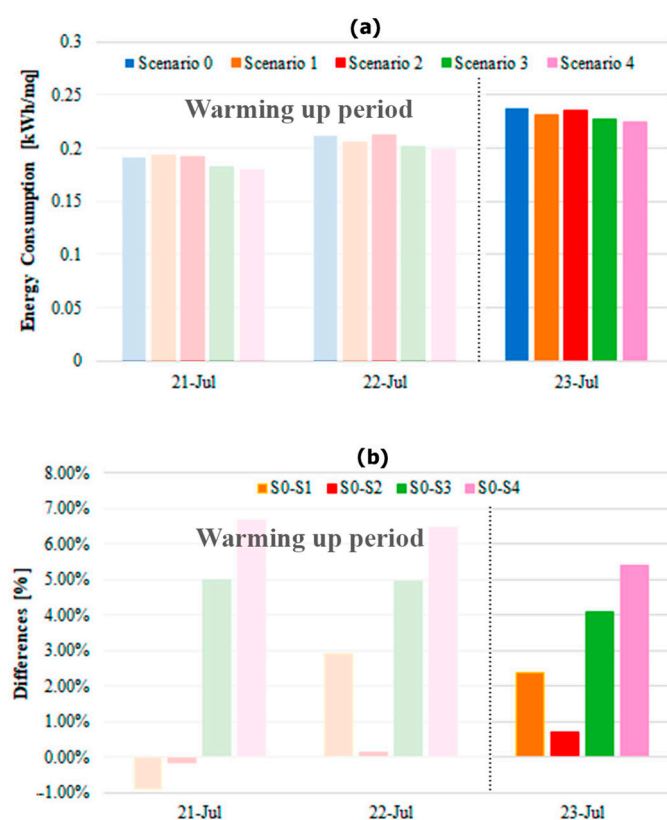


**Figure 21.** (**a**) Daily cooling energy consumption and (**b**) daily percentage differences in cooling energy consumption of all scenarios (S2 shows similar cooling energy consumption as in S0; S4 performs best, followed by S3 and S1).

## 5. Discussion

The above-described outcomes highlight how the urban heat island effect and the local climate change result in a significant impact on both outdoor thermal comfort and buildings' energy consumption, respectively, discussed in the following subsections. It is worth noting that these are the key topics of this study; nevertheless, further specific aspects should be considered when an actual mitigation strategy is developed. For example, the economic and technical feasibility of each strategy could have a significant impact on the cost–benefit assessments. For example, on the one hand, green walls/roofs can be much more expensive than cool walls/roofs and can be harder to be implemented into existing walls. With this regard, a dedicated study conducted across the main Australian cities [64] found that—depending on the location considered—green walls can be implemented only on 3% or 34% of the considered existing envelopes. On the other hand, the overall

evaluation can be changed when ecological, real estate, and social benefits are included in the assessment [65]. This brief example underlines how considering all the direct and indirect benefits of these strategies can be extremely complex; it is a further step in the comparison of mitigation strategies which could start from the results of this study for future works, as was better described in Section 6.

### 5.1. Urban Heat Island Effect

Based on the conducted analyses, the air and surface temperature results of the baseline scenario are worthy of consideration. As previously demonstrated [22], the more detailed analysis carried out in this study confirm that one of the major causes of greater urban heat island intensity in Corso Cavour may be its geometric configuration. Outdoor comfort in the canyon is mainly affected by exposure to solar radiation and, accordingly, street orientation and the height/width ratio have a considerable effect [66]. The presence of tall buildings and narrow streets in the considered area creates urban canyons that, with the low sky view factor and limited surface emissivity, seem to favor heat accumulation because of the numerous urban-related obstacles. During the day, depending on the sun's position, the presence of buildings may ensure shading and lower temperatures in some limited areas; nevertheless, when the solar radiation reaches the canyon surfaces, the radiation is absorbed and thus retained, increasing the temperatures. The simulation also demonstrated that the UHI configuration is affected by the wind's direction and speed, whose path is influenced by the buildings, reducing the convection-driven heat dissipation. Moreover, urban materials influence solar absorption and reflection; indeed, the area of Corso Cavour mainly consists of asphalt and concrete, materials with low solar reflectance indexes. Hence, most of the solar radiation is absorbed, contributing to the rise in temperatures ($T_{Air}$ > 32 °C and $T_{Surface}$ > 55.0 °C on streets at 12:00 p.m.). This assumption is confirmed by the high temperatures recorded at night when urban canyons slow down the cooling because the urban fabric of buildings prevent heat release. Furthermore, on the one hand, Corso Cavour is a densely populated and busy area, and the high contribution of the anthropogenic heat can worsen the UHI effect. On the other hand, the vegetation is poorly present in this area, limiting the beneficial contributions of direct shading and evapotranspiration. Indeed, at 12:00 p.m., the few areas directly shaded by trees recorded surface temperatures lower than the surrounding areas, being up to 10 °C cooler.

Once the starting point and the initial microclimatic conditions of Scenario 0 are defined, further considerations on the tested mitigation technologies can be conducted. As expected, the baseline exhibits the highest air temperatures while implementing green walls, which seems to be the most efficient strategy for UHI mitigation, followed by green roofs, cool roofs, and cool walls. Indeed, based on the obtained results, all the mitigation strategies adopted in this study are beneficial and mitigate temperatures even if some prove to be more effective than others.

The analyses conducted show that the implementation of green roofs can decrease the air temperature by up to 0.5 °C in the considered period while the benefits on the surface temperature are limited because the green roofs are realized at a different height compared to the analysis grid (located at 1.5 m above the ground). On the contrary, adopting green walls can reduce both the air temperature (differences up to 1.3 °C compared to the baseline model) and the surface temperature (up to 1 °C) mainly for the secondary roads where the green walls are closer to the analysis grid.

Comparing the effectiveness of these two types of green envelopes (Scenario 1 and Scenario 2), green roofs provide overall benefits; nevertheless, their effect is maximized close to the roofs, which are far from the analysis grid in a high-rise area. On the contrary, green walls perform better within the canyon as they reduce surface temperatures that play an important role in the definition of the canyon's microclimate. The combination of the decrease in surface and air temperature offered by green walls leads to better outdoor thermal comfort conditions. From a thermal point of view, green roofs can affect the overall urban air temperature, although they only slightly improve the pedestrian thermal comfort

due to their lower impact within the urban canyon. Furthermore, as demonstrated by Alexandri E. and Jones P. [33], the wider the canyon, the weaker is the effect of green roofs and green walls on temperature decrease. This theoretical concept has also been confirmed in our study, where the mitigation effect is generally greater along secondary roads than along the main street (Corso Cavour). In wider canyons, temperatures are dominated by the larger street surface and their greater exposure to direct solar radiation, while narrow canyons are primarily affected by solar reflection on walls and the shading effect; for this reason, the green walls allow for better performances. It was also demonstrated [67] that in cities with regular building block arrays, like Corso Cavour, if the greenery is parallel to the wind path, the effects of temperature reduction are greater. In fact, for the green wall strategy (Scenario 2), the roads in the East–West direction—the same direction of the summer prevailing winds—show more beneficial mitigation effects.

Adopting cool materials on roofs (Scenario 3) and walls (Scenario 4) shows almost the same temperature trend. Regarding the air temperature, the hourly and daily temperature averages of the two mitigation scenarios are almost identical, showing the same differences compared to the baseline. The highest benefits considering air temperatures are shown in the late evening: in the hottest hours, air temperatures show almost constant differences of 0.2–0.4 °C, which increase up to 0.5 °C in the evening hours. On the contrary, the differences are negative in the early hours of the day (between −0.3 °C and −0.1 °C). A similar effect is also observed for surface temperatures: the temperature variations are very similar between Scenario 3 and Scenario 4, although cool walls generally show slightly lower temperatures along secondary roads. Thus, according to the simulation results, cool walls and roofs with an albedo value of 0.69 show similar temperature reductions. Moreover, the reduction in air temperatures in cool envelope scenarios is less impactful than green envelope strategies; however, as demonstrated in several studies [40,42], the insertion of cool materials inside cities still brings benefits.

### 5.2. Implications on the Building Energy Consumption

With reference to the energy consumption analyses, the baseline (Scenario 0) is still the most disadvantaged scenario, while cool walls (Scenario 4) and cool roofs (Scenario 3) are the most energy-efficient mitigation strategies, followed by green roofs (Scenario 1) and green walls (Scenario 2). However, all the scenarios show positive results, and it is worth noting that the energy scenarios are linked to the respective mitigation scenarios. Indeed, the results obtained are derived from the combination of changes in the urban microclimate and mitigation technologies on buildings. Therefore, apart from Scenario 0, the climate files adopted are characterized by lower outdoor temperatures, resulting from the UHI mitigation effects of the different technologies applied at urban scale.

Regardless of the scenario considered, the results show that the highest consumptions are referred to the southwest thermal zones, while the lowest are recorded in the northern ones. This trend can be easily explained considering that the simulations were conducted during the summer period and that the southwest exposure is the most exposed to solar radiation during the hottest hours of the day while the northern ones are not exposed to direct solar radiation.

The cooling system starts operating from 10:00 a.m., and between 10:00 a.m. and 11:00 a.m. there is an initial peak of energy demand in all zones due to the heat stored during the previous hours when the system is off. Such consumption decreases in the following two hours and rises between 7:00 p.m. and 8:00 p.m. This generally occurs for all the three days simulated; according to the air temperature data collected, in these hours, the increase in cooling demand coincides with an increase in the outdoor air temperature.

Many studies [68,69] have underlined the effectiveness of using green walls in mitigating the UHI effect and reducing cooling consumption. In this study, the data show that the southwestern thermal zones are those that mostly benefit from the application of green walls, with a saving rate of up to 2.5%, while northern and northeastern thermal zone consumptions worsen compared to Scenario 0. This could be due to the lower incident

solar radiation which reduces the evapotranspiration mechanism of the plant mantle [33]; this the reason why this type of technology is usually applied on south-facing facades. The lack of this contribution, combined with a green wall albedo value (0.2) lower than the one adopted in the baseline (0.5), leads to average differences in energy consumption of −0.16% both in the northeast thermal zones. The results of the total sum of consumption for building cooling show that Scenario 2 is the most penalized, with a reduction in total consumption limited to only 1.7%.

A study by Zinzi and Agnoli [70] demonstrated that cool and green roofs are very effective for cooling and energy-saving. Nevertheless, cool roofs are more effective than green roofs for southern Mediterranean areas because—relying on rainfall—during the dry Mediterranean hot season, the green roofs are not wet enough to guarantee good cooling performances. The results obtained in our analyses confirm this trend as, compared to Scenario 0, the green roofs show a total reduction of 2.3% for cooling consumption against almost the 4.0% registered in the cool roofs scenario.

Moving to the last mitigation strategy, the results showed that from an energy point of view, the adoption of cool walls brings the greatest benefits. Overall, during the last simulated day, the energy-savings related to the cool walls were higher than 5.3% compared to the baseline scenario followed by cool roofs (4%), green roofs (nearly 2.3%), and green walls (0.7%).

## 6. Conclusions

Urban climate simulations and dynamic energy analyses of a residential building have contributed to defining UHI mitigation and energy-saving potential by adopting innovative envelope technologies. Firstly, the results show that both the urban microclimate and the building consumption are affected by the mitigation strategies considered even in a small urban area. From a microclimate point of view, the use of green façades proved to be the most effective in reducing air temperatures in the urban canyons while green roofs, cool roofs, and cool walls progressively showed lower efficacies. Instead, from a building perspective, the best performances were recorded for the cool walls scenario, while cool roofs, green roofs, and green walls progressively reduced the energy-saving benefits. It is worth noting that the most effective strategy from an urban point of view (green walls) is the worst from a building perspective and, vice versa, the highest energy savings (cool walls) correspond to the lowest urban microclimate benefits. Similarly, the intermediate strategies also show a reversed behavior. This trend highlights the importance of assessing both microclimate and building behavior to find the best trade off according to the specific case study. Future studies could be focused on this topic by conducting a multi-objective optimization to find a set of optimal solutions to improve both urban microclimate and building consumptions; nevertheless, the main issue would probably be the high computational demand related to the urban microclimate simulations in the optimization loop. Furthermore, this paper has evaluated the benefits of UHI mitigation strategies in terms of outdoor thermal comfort and building energy consumption; nevertheless, when no cooling systems are implemented, the effects of the mitigation strategies on the indoor thermal comfort can play a pivotal role for the users' comfort. This topic is particularly interesting for several vulnerable groups of the population that are strongly affected by the mitigation strategies; therefore, this topic deserves further investigations in future studies.

Finally, it is worth highlighting the limitations of this study to properly interpret the results and to allow for consistent future further studies. In particular, from a modeling point of view, the use of a commercial software (ENVI-met) reduces the replicability of these analyses; nevertheless, the wide application of this tool allows for a good comparability of the results with other studies. Furthermore, this study is mainly focused on the thermal and energy benefits of the mitigation strategies while their social, economic, and technological feasibility are out of the scope of this work. Undoubtedly, this topic can be the starting point for a subsequent study which considers the capital cost and maintenance requirement of each analyzed technology comparing them with the results of this paper during the whole

building life cycle to quantify their economic feasibility. Moreover, the technical feasibility can also be considered to account exactly the type and number of existing buildings and areas which can be equipped with the mitigation technologies analyzed. Finally, the social benefits and the real estate value can also be considered in an overall assessment of the benefits related to each strategy. Hence, technical, social, and economic insights would all provide a feasibility study complementary to this paper.

In conclusion, a combined analysis involving microclimate modeling and energy simulations allowed us to assess the simultaneous benefits of mitigation technologies from both urban and building perspectives. Despite the impossibility of modeling the entire city and the limited simulation period considered, the results could help to obtain a screening of the mitigation technologies to be adopted in a Mediterranean area to select the ones to be implemented and tested.

## References

1. *IPCC Climate Change 2022: Impacts, Adaptation and Vulnerability*; Contribution of Working Group II to the Sixth Assessment Report of the Intergovernmental Panel on Climate Change; Cambridge University Press: Cambridge, UK, 2022.
2. Santamouris, M. On the Energy Impact of Urban Heat Island and Global Warming on Buildings. *Energy Build.* **2014**, *82*, 100–113. [CrossRef]
3. De Sherbinin, A.; Schiller, A.; Pulsipher, A. The vulnerability of global cities to climate hazards. *Environ. Urban.* **2007**, *19*, 39–64. [CrossRef]
4. Urban Adaptation in Europe. European Environment Agency. Available online: https://www.eea.europa.eu/publications/urban-adaptation-in-europe (accessed on 9 May 2024).
5. Tapia, C.; Abajo, B.; Feliu, E.; Mendizabal, M.; Martinez, J.A.; Fernández, J.G.; Laburu, T.; Lejarazu, A. Profiling Urban Vulnerabilities to Climate Change: An Indicator-Based Vulnerability Assessment for European Cities. *Ecol. Indic.* **2017**, *78*, 142–155. [CrossRef]
6. Lehner, F.; Deser, C.; Sanderson, B.M. Future Risk of Record-Breaking Summer Temperatures and Its Mitigation. *Clim. Chang.* **2018**, *146*, 363–375. [CrossRef]
7. Guerreiro, S.B.; Dawson, R.J.; Kilsby, C.; Lewis, E.; Ford, A. Future Heat-Waves, Droughts and Floods in 571 European Cities. *Environ. Res. Lett.* **2018**, *13*, 034009. [CrossRef]
8. Lauwaet, D.; De Ridder, K.; Saeed, S.; Brisson, E.; Chatterjee, F.; van Lipzig, N.P.M.; Maiheu, B.; Hooyberghs, H. Assessing the Current and Future Urban Heat Island of Brussels. *Urban. Clim.* **2016**, *15*, 1–15. [CrossRef]
9. Santamouris, M. Analyzing the Heat Island Magnitude and Characteristics in One Hundred Asian and Australian Cities and Regions. *Sci. Total Environ.* **2015**, *512–513*, 582–598. [CrossRef]
10. Santamouris, M. Recent Progress on Urban Overheating and Heat Island Research. Integrated Assessment of the Energy, Environmental, Vulnerability and Health Impact. Synergies with the Global Climate Change. *Energy Build.* **2020**, *207*, 109482. [CrossRef]
11. Akbari, H.; Cartalis, C.; Kolokotsa, D.; Muscio, A.; Pisello, A.L.; Rossi, F.; Santamouris, M.; Synnefa, A.; Wong, N.H.; Zinzi, M. Local Climate Change and Urban Heat Island Mitigation Techniques—The State of the Art. *J. Civil. Eng. Manag.* **2016**, *22*, 1–16. [CrossRef]
12. He, B.-J.; Zhao, D.; Xiong, K.; Qi, J.; Ulpiani, G.; Pignatta, G.; Jones, P. A framework for addressing urban heat challenges and associated adaptive behavior by the public and the issue of willingness to pay for heat resilient infrastructure in Chongqing, China. *Sustain. Cities Soc.* **2021**, *75*, 103361. [CrossRef]
13. Escandón, R.; Suárez, R.; Sendra, J.J. Field Assessment of Thermal Comfort Conditions and Energy Performance of Social Housing: The Case of Hot Summers in the Mediterranean Climate. *Energy Policy* **2019**, *128*, 377–392. [CrossRef]
14. Santamouris, M. Regulating the Damaged Thermostat of the Cities—Status, Impacts and Mitigation Challenges. *Energy Build.* **2015**, *91*, 43–56. [CrossRef]

15. Adaptation Challenges and Opportunities for the European Energy System. European Environment Agency. Available online: https://www.eea.europa.eu/publications/adaptation-in-energy-system (accessed on 9 May 2024).

16. Liu, C.; Kershaw, T.; Fosas, D.; Ramallo Gonzalez, A.P.; Natarajan, S.; Coley, D.A. High Resolution Mapping of Overheating and Mortality Risk. *Build. Environ.* **2017**, *122*, 1–14. [CrossRef]

17. Irfeey, A.M.M.; Chau, H.W.; Sumaiya, M.M.F.; Wai, C.Y.; Muttil, N.; Jamei, E. Sustainable Mitigation Strategies for Urban Heat Island Effects in Urban Areas. *Sustainability* **2023**, *15*, 10767. [CrossRef]

18. Akbari, H.; Kolokotsa, D. Three Decades of Urban Heat Islands and Mitigation Technologies Research. *Energy Build.* **2016**, *133*, 834–842. [CrossRef]

19. Calliari, E.; Staccione, A.; Mysiak, J. An Assessment Framework for Climate-Proof Nature-Based Solutions. *Sci. Total Environ.* **2019**, *656*, 691–700. [CrossRef]

20. Battista, G.; de Lieto Vollaro, E.; Ocłoń, P.; de Lieto Vollaro, R. Effects of Urban Heat Island Mitigation Strategies in an Urban Square: A Numerical Modelling and Experimental Investigation. *Energy Build.* **2023**, *282*, 112809. [CrossRef]

21. U.S. Environmental Protection Agencys Office of Atmospheric Programs. Reducing Urban Heat Islands: Compendium of Strategies—Urban Heat Island Basics. Available online: https://www.epa.gov/sites/default/files/2017-05/documents/reducing_urban_heat_islands_ch_5.pdf (accessed on 9 May 2024).

22. Martinelli, A.; Kolokotsa, D.D.; Fiorito, F. Urban Heat Island in Mediterranean Coastal Cities: The Case of Bari (Italy). *Climate* **2020**, *8*, 79. [CrossRef]

23. Li, X.; Zhou, Y.; Yu, S.; Jia, G.; Li, H.; Li, W. Urban Heat Island Impacts on Building Energy Consumption: A Review of Approaches and Findings. *Energy* **2019**, *174*, 407–419. [CrossRef]

24. Akbari, H.; Davis, S.; Huang, J.; Dorsano, S.; Winnett, S. Cooling Our Communities. A Guidebook on Tree Planting and Light-Colored Surfacing. *EScholarship* **2009**. [CrossRef]

25. Santamouris, M.; Papanikolaou, N.; Livada, I.; Koronakis, I.; Georgakis, C.; Argiriou, A.; Assimakopoulos, D.N. On the Impact of Urban Climate on the Energy Consumption of Buildings. *Sol. Energy* **2001**, *70*, 201–216. [CrossRef]

26. De Cian, E.; Pavanello, F.; Randazzo, T.; Mistry, M.N.; Davide, M. Households' Adaptation in a Warming Climate. Air Conditioning and Thermal Insulation Choices. *Environ. Sci. Policy* **2019**, *100*, 136–157. [CrossRef]

27. Pyrgou, A.; Castaldo, V.L.; Pisello, A.L.; Cotana, F.; Santamouris, M. On the Effect of Summer Heatwaves and Urban Overheating on Building Thermal-Energy Performance in Central Italy. *Sustain. Cities Soc.* **2017**, *28*, 187–200. [CrossRef]

28. Taylor, J.; Wilkinson, P.; Picetti, R.; Symonds, P.; Heaviside, C.; Macintyre, H.L.; Davies, M.; Mavrogianni, A.; Hutchinson, E. Comparison of Built Environment Adaptations to Heat Exposure and Mortality during Hot Weather, West Midlands Region, UK. *Environ. Int.* **2018**, *111*, 287–294. [CrossRef] [PubMed]

29. Baldinelli, G.; Bonafoni, S.; Anniballe, R.; Presciutti, A.; Gioli, B.; Magliulo, V. Spaceborne Detection of Roof and Impervious Surface Albedo: Potentialities and Comparison with Airborne Thermography Measurements. *Sol. Energy* **2015**, *113*, 281–294. [CrossRef]

30. European Commission. Towards an EU Research and Innovation Policy Agenda for Nature-Based Solutions & Re-Naturing Cities. 2015. Available online: https://op.europa.eu/en/publication-detail/-/publication/fb117980-d5aa-46df-8edc-af367cddc202/language-en (accessed on 9 May 2024).

31. Ihobe Environmental Management Agency Nature-Based Solutions for Local Climate Adaptation in the Basque Country Methodological Guide for Their Identification and Mapping. Donostia/San Sebastián Case Study. 2017. Available online: https://growgreenproject.eu/wp-content/uploads/2018/05/NBS-Climate-Adaptation-Basque-Country.pdf (accessed on 9 May 2024).

32. Wong, N.H.; Tan, A.Y.K.; Tan, P.Y.; Sia, A.; Wong, N.C. Perception Studies of Vertical Greenery Systems in Singapore. *J. Urban. Plan. Dev. Asce* **2010**, *136*, 330–338. [CrossRef]

33. Alexandri, E.; Jones, P. Temperature Decreases in an Urban Canyon Due to Green Walls and Green Roofs in Diverse Climates. *Build. Environ.* **2008**, *43*, 480–493. [CrossRef]

34. Djedjig, R.; Bozonnet, E.; Belarbi, R. Modeling Green Wall Interactions with Street Canyons for Building Energy Simulation in Urban Context. *Urban. Clim.* **2016**, *16*, 75–85. [CrossRef]

35. Brahimi, M.; Benabbas, M.; Altan, H.; Nocera, F.; Costanzo, V. Enhancing Urban Microclimates: Potential Benefits of Greenery Strategies in a Semi-Arid Environment. *Sustainability* **2023**, *15*, 16380. [CrossRef]

36. Santamouris, M.; Ding, L.; Fiorito, F.; Oldfield, P.; Osmond, P.; Paolini, R.; Prasad, D.; Synnefa, A. Passive and Active Cooling for the Outdoor Built Environment—Analysis and Assessment of the Cooling Potential of Mitigation Technologies Using Performance Data from 220 Large Scale Projects. *Sol. Energy* **2017**, *154*, 14–33. [CrossRef]

37. Susca, T.; Zanghirella, F.; Colasuonno, L.; Del Fatto, V. Effect of Green Wall Installation on Urban Heat Island and Building Energy Use: A Climate-Informed Systematic Literature Review. *Renew. Sustain. Energy Rev.* **2022**, *159*, 112100. [CrossRef]

38. Djedjig, R.; Belarbi, R.; Bozonnet, E. Green Wall Impacts inside and Outside Buildings: Experimental Study. *Energy Procedia* **2017**, *139*, 578–583. [CrossRef]

39. Yang, X.; Yao, L.; Peng, L.L.H. Impacts of Urban Air Temperature and Humidity on Building Cooling and Heating Energy Demand in 15 Cities of Eastern China. *Energy* **2024**, *288*, 129887. [CrossRef]

40. Santamouris, M. Cooling the Cities—A Review of Reflective and Green Roof Mitigation Technologies to Fight Heat Island and Improve Comfort in Urban Environments. *Sol. Energy* **2014**, *103*, 682–703. [CrossRef]

41. Falasca, S.; Ciancio, V.; Salata, F.; Golasi, I.; Rosso, F.; Curci, G. High Albedo Materials to Counteract Heat Waves in Cities: An Assessment of Meteorology, Buildings Energy Needs and Pedestrian Thermal Comfort. *Build. Environ.* **2019**, *163*, 106242. [CrossRef]

42. Kolokotsa, D.D.; Giannariakis, G.; Gobakis, K.; Giannarakis, G.; Synnefa, A.; Santamouris, M. Cool Roofs and Cool Pavements Application in Acharnes, Greece. *Sustain. Cities Soc.* **2018**, *37*, 466–474. [CrossRef]

43. Hosseini, M.; Akbari, H. Effect of Cool Roofs on Commercial Buildings Energy Use in Cold Climates. *Energy Build.* **2016**, *114*, 143–155. [CrossRef]

44. Coccolo, S.; Kämpf, J.; Mauree, D.; Scartezzini, J.L. Cooling Potential of Greening in the Urban Environment, a Step Further towards Practice. *Sustain. Cities Soc.* **2018**, *38*, 543–559. [CrossRef]

45. Nazarian, N.; Dumas, N.; Kleissl, J.; Norford, L. Effectiveness of Cool Walls on Cooling Load and Urban Temperature in a Tropical Climate. *Energy Build.* **2019**, *187*, 144–162. [CrossRef]

46. Yang, X.; Chen, Y.; Peng, L.L.H.; Wang, Q. Quantitative Methods for Identifying Meteorological Conditions Conducive to the Development of Urban Heat Islands. *Build. Environ.* **2020**, *178*, 106953. [CrossRef]

47. Elmarakby, E.; Elkadi, H. Impact of Urban Morphology on Urban Heat Island in Manchester's Transit-Oriented Development. *J. Clean. Prod.* **2024**, *434*, 140009. [CrossRef]

48. Tsoka, S.; Tsikaloudaki, A.; Theodosiou, T. Analyzing the ENVI-Met Microclimate Model's Performance and Assessing Cool Materials and Urban Vegetation Applications–A Review. *Sustain. Cities Soc.* **2018**, *43*, 55–76. [CrossRef]

49. Ouyang, W.; Sinsel, T.; Simon, H.; Morakinyo, T.E.; Liu, H.; Ng, E. Evaluating the Thermal-Radiative Performance of ENVI-Met Model for Green Infrastructure Typologies: Experience from a Subtropical Climate. *Build. Environ.* **2022**, *207*, 108427. [CrossRef]

50. Crank, P.J.; Sailor, D.J.; Ban-Weiss, G.; Taleghani, M. Evaluating the ENVI-Met Microscale Model for Suitability in Analysis of Targeted Urban Heat Mitigation Strategies. *Urban Clim.* **2018**, *26*, 188–197. [CrossRef]

51. Ayyad, Y.N.; Sharples, S. Envi-MET Validation and Sensitivity Analysis Using Field Measurements in a Hot Arid Climate. *IOP Conf. Ser. Earth Environ. Sci.* **2019**, *329*, 012040. [CrossRef]

52. ENVI-Met QUICKSTART. Available online: https://www.envi-met.com/ (accessed on 9 May 2024).

53. Zhang, Y.; Hu, X.; Cao, X.; Liu, Z. Numerical Simulation of the Thermal Environment during Summer in Coastal Open Space and Research on Evaluating the Cooling Effect: A Case Study of May Fourth Square, Qingdao. *Sustainability* **2022**, *14*, 15126. [CrossRef]

54. Cortes, A.; Rejuso, A.J.; Santos, J.A.; Blanco, A. Evaluating Mitigation Strategies for Urban Heat Island in Mandaue City Using ENVI-Met. *J. Urban. Manag.* **2022**, *11*, 97–106. [CrossRef]

55. Taleb, D.; Abu-Hijleh, B. Urban Heat Islands: Potential Effect of Organic and Structured Urban Configurations on Temperature Variations in Dubai, UAE. *Renew. Energy* **2013**, *50*, 747–762. [CrossRef]

56. Ng, E.; Chen, L.; Wang, Y.; Yuan, C. A Study on the Cooling Effects of Greening in a High-Density City: An Experience from Hong Kong. *Build. Environ.* **2012**, *47*, 256–271. [CrossRef]

57. Yilmaz, S.; Kurt, A.; GÖLCÜ, M. ENVI-Met Simulations of the Effect of Different Landscape Design Scenarios on Pedestrian Thermal Comfort: Haydar Aliyev Street. *Yüzüncü Yıl Üniversitesi Tarım Bilim. Derg.* **2023**, *33*, 338–353. [CrossRef]

58. Middel, A.; Häb, K.; Brazel, A.J.; Martin, C.A.; Guhathakurta, S. Impact of Urban Form and Design on Mid-Afternoon Microclimate in Phoenix Local Climate Zones. *Landsc. Urban. Plan.* **2014**, *122*, 16–28. [CrossRef]

59. Ambrosini, D.; Galli, G.; Mancini, B.; Nardi, I.; Sfarra, S. Evaluating Mitigation Effects of Urban Heat Islands in a Historical Small Center with the ENVI-Met® Climate Model. *Sustainability* **2014**, *6*, 7013–7029. [CrossRef]

60. Yang, X.; Zhao, L.; Bruse, M.; Meng, Q. Evaluation of a Microclimate Model for Predicting the Thermal Behavior of Different Ground Surfaces. *Build. Environ.* **2013**, *60*, 93–104. [CrossRef]

61. Sen, S.; Roesler, J. Aging Albedo Model for Asphalt Pavement Surfaces. *J. Clean. Prod.* **2016**, *117*, 169–175. [CrossRef]

62. Lontorfos, V.; Efthymiou, C.; Santamouris, M. On the Time Varying Mitigation Performance of Reflective Geoengineering Technologies in Cities. *Renew. Energy* **2018**, *115*, 926–930. [CrossRef]

63. *Ministry of Economic Development Ministerial Decree 26/06/2015, Calculation Methodologies of the Building Energy Performance and Minimum Requirements for Buildings*; 2015; pp. 1–8.

64. Douglas, A.N.J.; Morgan, A.L.; Rogers, E.I.E.; Irga, P.J.; Torpy, F.R. Evaluating and Comparing the Green Wall Retrofit Suitability across Major Australian Cities. *J. Environ. Manag.* **2021**, *298*, 113417. [CrossRef] [PubMed]

65. Teotónio, I.; Silva, C.M.; Cruz, C.O. Economics of Green Roofs and Green Walls: A Literature Review. *Sustain. Cities Soc.* **2021**, *69*, 102781. [CrossRef]

66. Vallati, A.; Mauri, L.; Colucci, C. Impact of Shortwave Multiple Reflections in an Urban Street Canyon on Building Thermal Energy Demands. *Energy Build.* **2018**, *174*, 77–84. [CrossRef]

67. Tan, Z.; Lau, K.K.L.; Ng, E. Urban Tree Design Approaches for Mitigating Daytime Urban Heat Island Effects in a High-Density Urban Environment. *Energy Build.* **2016**, *114*, 265–274. [CrossRef]

68. Assimakopoulos, M.N.; De Masi, R.F.; de Rossi, F.; Papadaki, D.; Ruggiero, S. Green Wall Design Approach Towards Energy Performance and Indoor Comfort Improvement: A Case Study in Athens. *Sustainability* **2020**, *12*, 3772. [CrossRef]

69. Coma, J.; Pérez, G.; de Gracia, A.; Burés, S.; Urrestarazu, M.; Cabeza, L.F. Vertical Greenery Systems for Energy Savings in Buildings: A Comparative Study between Green Walls and Green Facades. *Build. Environ.* **2017**, *111*, 228–237. [CrossRef]

70. Zinzi, M.; Agnoli, S. Cool and Green Roofs. An Energy and Comfort Comparison between Passive Cooling and Mitigation Urban Heat Island Techniques for Residential Buildings in the Mediterranean Region. *Energy Build.* **2012**, *55*, 66–76. [CrossRef]